Journal of the American Heart Association

ORIGINAL RESEARCH

Identification of Genes and Pathways Regulated by Lamin A in Heart

Jordi Coste Pradas, MS; Gaelle Auguste, PhD; Scot J. Matkovich, PhD; Raffaella Lombardi, MD, PhD; Suet Nee Chen, PhD; Tyrone Garnett, BS; Kyle Chamberlain, PhD; Jalish Mahmud Riyad, MS; Thomas Weber, PhD; Sanjay K. Singh, PhD; Matthew J. Robertson, PhD; Cristian Coarfa, PhD; Ali J. Marian, MD; Priyatansh Gurha, PhD

BACKGROUND: Mutations in the *LMNA* gene, encoding LMNA (lamin A/C), causes distinct disorders, including dilated cardiomyopathies, collectively referred to as laminopathies. The genes (coding and noncoding) and regulatory pathways controlled by LMNA in the heart are not completely defined.

METHODS AND RESULTS: We analyzed cardiac transcriptome from wild-type, loss-of-function (*Lmna*$^{-/-}$), and gain-of-function (*Lmna*$^{-/-}$ injected with adeno-associated virus serotype 9 expressing LMNA) mice with normal cardiac function. Deletion of *Lmna* (*Lmna*$^{-/-}$) led to differential expression of 2193 coding and 629 long noncoding RNA genes in the heart (q<0.05). Re-expression of LMNA in the *Lmna*$^{-/-}$ mouse heart, completely rescued 501 coding and 208 non-coding and partially rescued 1862 coding and 607 lncRNA genes. Pathway analysis of differentially expressed genes predicted activation of transcriptional regulators lysine-specific demethylase 5A, lysine-specific demethylase 5B, tumor protein 53, and suppression of retinoblastoma 1, paired-like homeodomain 2, and melanocyte-inducing transcription factor, which were completely or partially rescued upon reexpression of LMNA. Furthermore, lysine-specific demethylase 5A and 5B protein levels were increased in the *Lmna*$^{-/-}$ hearts and were partially rescued upon LMNA reexpression. Analysis of biological function for rescued genes identified activation of tumor necrosis factor-α, epithelial to mesenchymal transition, and suppression of the oxidative phosphorylation pathway upon *Lmna* deletion and their restoration upon LMNA reintroduction in the heart. Restoration of the gene expression and transcriptional regulators in the heart was associated with improved cardiac function and increased survival of the *Lmna*$^{-/-}$ mice.

CONCLUSIONS: The findings identify LMNA-regulated cardiac genes and their upstream transcriptional regulators in the heart and implicate lysine-specific demethylase 5A and B as epigenetic regulators of a subset of the dysregulated genes in laminopathies.

Key Words: cardiomyopathies ■ KDM5 ■ laminopathies ■ LMNA

Mutations in the *LMNA* gene, encoding LMNA (lamin A/C), cause a diverse array of phenotypes involving multiple organs that are collectively referred to as laminopathies.[1–4] Notable among the laminopathies are dilated cardiomyopathy (DCM), cardiac conduction defects, arrhythmias, Hutchinson-Gilford progeria syndrome, Emery-Dreifuss muscular dystrophy, and familial partial lipodystrophy.[1–6] *LMNA* is among the most common causal genes for hereditary DCM, accounting for 6% to 8% of familial DCM and for a small fraction of arrhythmogenic cardiomyopathy.[2,5,6] DCM is the major cause of death in a subset of laminopathies involving striated muscles and typically manifests with conduction defects, arrhythmias,

Correspondence to: Priyatansh Gurha, PhD, Brown Foundation Institute of Molecular Medicine, The University of Texas Health Sciences Center, Center for Cardiovascular Genetics, 6770 Bertner Street, Suite C950G, Houston, TX 77030. E-mail: priyatansh.gurha@uth.tmc.edu

Supplementary Materials for this article are available at https://www.ahajournals.org/doi/suppl/10.1161/JAHA.119.015690

Raffaella Lombardi is currently located at the Division of Cardiology, Department of Advanced Biomedical Science, University of Naples Federico II, Italy.

Suet Nee Chen is currently located at the CU-Cardiovascular Institute and Adult Medical Genetics Program, University of Colorado Anschutz Medical Campus, Aurora, CO.

For Sources of Funding and Disclosures, see page 16.

JAHA is available at: www.ahajournals.org/journal/jaha

CLINICAL PERSPECTIVE

What Is New?

- Genetic deletion of the *Lmna* gene, encoding LMNA (lamin A/C) protein, was associated with dysregulation of several thousand coding and noncoding genes in the heart and led to myocardial fibrosis, apoptosis, cardiac dysfunction, and premature death.
- Genes whose expression levels were dysregulated predicted activation or suppression of over 2 dozen transcriptional regulators, including histone demethylases lysine-specific demethylase 5A and B.
- Reexpression of LMNA, predominantly in cardiac myocytes using recombinant adeno-associated virus serotype 9 constructs, in the *Lmna*-deficient mice normalized or partially restored expression levels of a few thousand genes, including targets of the lysine-specific demethylase 5A and B, and restoration of gene expression in the heart was associated with improved cardiac function and prolonged survival.

What Are the Clinical Implications?

- The findings by unraveling putative pathogenic transcriptional regulators of cardiac phenotypes in laminopathies, including lysine-specific demethylase 5A and B, provide for potential therapeutic targets in heart failure caused by the *LMNA* mutations.

Nonstandard Abbreviations and Acronyms

AAV9	adeno-associated virus serotype 9
DAPI	4′,6-diamidino-2-phenylindole
DCM	dilated cardiomyopathy
GSEA	gene set enrichment analysis
IPA	Ingenuity Pathway Analysis
KDM5A	lysine-specific demethylase 5A
KDM5B	lysine-specific demethylase 5B
LADs	lamina-associated domains
limma	linear models for microarray data
LMNA	lamin A
MAPK4	mitogen-activated protein kinase 4
PCM1	pericentriolar material-1
PITX2	paired-like homeodomain 2
RB1	retinoblastoma 1
TGF	transforming growth factor-β1
TP53	tumor protein 53
TR	transcriptional regulator
WT	wild-type

and cardiac dysfunction.[7,8] Accordingly, patients with *LMNA* mutations are at a high risk of sudden cardiac death, which typically necessitates implantation of a defibrillator/pacemaker.[7,8]

LMNA is expressed in differentiated cells, including cardiac myocytes. Within the nucleus, lamin and associated proteins form a fibrous multiprotein network termed as nuclear lamina that lines the nucleoplasmic face of the inner nuclear membrane. Genomic regions that are in close contact with the nuclear lamina are known as lamina-associated domains (LADs).[9–12] LMNA through LAD plays an important role in spatial chromatin organization and gene expression. Genes within LADs are expressed at low levels and are depleted for active histone marks like H3K4me3.[9–12] Recently, we identified over 300 LADs in human cardiac myocytes, encompassing several thousand coding and noncoding genomic regions. We further demonstrated that LADs are redistributed in DCM, and this redistribution affects gene expression either directly or indirectly.[13]

The molecular pathogenesis of DCM in laminopathies is not well understood; however, a large number of genes and pathways are found to be dysregulated, correlating with the phenotypic diversity of the *LMNA* mutations.[9,11,13–16] Defects in several signaling pathways, such as those including forkhead box O and MAPK4 (mitogen-activated protein kinase 4), have been implicated in the pathogenesis of DCM in laminopathies.[4,14,17,18] In addition, altered nuclear membrane mechanical integrity and DNA damage have emerged as putative mechanisms in the pathogenesis of laminopathies, including DCM.[19–22] However, the role of LMNA in regulating coding and noncoding genes, occurring before and independent of cardiac dysfunction, is not well understood. The present study is designed to bridge this knowledge gap by utilizing *Lmna* loss-of-function ($Lmna^{-/-}$) and partial gain-of-function mouse models. The latter were generated upon reexpression of wild-type (WT) LMNA in the heart in $Lmna^{-/-}$ mice using recombinant adeno-associated viruses (henceforth referred to as $Lmna^{-/-}$:AAV9-$Lmna^{WT}$).

We sequenced ribosomal-depleted RNA samples, extracted from whole hearts of WT and $Lmna^{-/-}$ mice when cardiac function was normal to reduce potential confounding effects of cardiac dysfunction on gene expression. To complement the findings, we reexpressed LMNA in the $Lmna^{-/-}$ hearts using recombinant AAV9 viruses and determined the ensuing transcriptomic changes in the heart at the same age. Comparing gene expression in the WT, $Lmna^{-/-}$ and $Lmna^{-/-}$:AAV9-$Lmna^{WT}$ hearts, we identified coding and noncoding genes whose expression was regulated by LMNA in the absence of cardiac dysfunction. Differentially expressed genes (DEGs) were used to

predict dysregulated activity of several transcriptional regulators (TRs), including lysine-specific demethylase 5A (KDM5A) and B, implicating them in the pathogenesis of DCM in laminopathies.

METHODS

Further details of the material and methods are provided in Data S1.

Mice

The phenotype of the *Lmna*$^{-/-}$ mice has been published.[17,20] *Lmna*$^{-/-}$ and WT littermates were used in these experiments, the latter as controls. List of oligonucleotide primers used for genotype screening is listed in Table S1.

Anesthesia and Euthanasia

Anesthesia was induced with 3% inhaled isoflurane and was maintained at 0.5% to 1% isoflurane inhalation throughout the procedure. Mice were euthanized by CO_2 inhalation followed by cervical dislocation. Animal studies were in accord with the NIH *Guide for the Care and Use of Laboratory Animals* published and approved by the Animal Care and Use Committee (AWC protocols: AWC-15-0052 and AWC-17-0146).

Echocardiography

Echocardiography was performed on mice anesthetized by intraperitoneal injection of sodium pentobarbital (60 mg/kg body weight). The mouse was positioned supine on a heating pad with embedded ECG leads. ECG and respiratory rate were recorded during the study. Wall thicknesses and left ventricular dimensions were measured from M-mode images in at least 3 cardiac cycles and the mean values were used. Left ventricular fractional shortening and mass were calculated as previously described.[17,23,24]

Immunoblotting

Immunoblotting was performed as published.[17,19,23] Nuclear protein isolation was performed using the nuclear extraction kit (Ab113474; Abcam, Cambridge, MA), and a 20- to 25-µg aliquot of each nuclear protein extract was used for immunoblotting analysis. The primary and secondary antibodies and their titers are listed in Table S2.

Immunofluorescence

Immunofluorescence staining to detect transgene expression and localization was performed as published.[17,19,23] In brief, thin myocardial cryosections, fixed in optimal cutting temperature (OCT), were incubated with an anti-Flag- LMNA or anti-pericentriolar material-1 (PCM1) antibody to detect expression of the transgenes within nuclei. The sections were counterstained with 4′,6-diamidino-2-phenylindole (DAPI) to identify the nuclei. Details of antibodies are presented in Table S2.

RNA Sequencing

Total RNA depleted of ribosomal RNA was used. RNA fragmentation, first- and second-strand cDNA synthesis (preserving strand information), and the addition of indexed adapters was carried out as previously described.[17,19,23,25] Paired-end, 100-bp reads were obtained on an HiSeq 4000 instrument (Illumina, San Diego, CA). Mapping of sequencing reads to the mouse genome GRCm38.91 (Ensembl) was performed using Tophat2.[26] The mean number of transcriptome-aligned reads per heart was 27.6 million. Read quantitation on a per-gene basis was performed with HTSeq[27] and the default gene annotation file (gtf) provided with the GRCm38.91 Ensembl genome distribution. Detectable RNAs were assessed as those present at or above 1 read per million (27 reads) in 50% of the samples, resulting in 15 096 RNAs for downstream analyses. Calculation of fold-change and false discovery rate for differentially expressed RNAs were obtained by the R/Bioconductor packages linear models for microarray data (limma) and edgeR/variance modeling at the observational level.[28] A batch correction was performed by including batch as a blocking factor in the linear model used by limma, per a published protocol.[28] To obtain quantitative read information for lncRNAs HTSeq was used together with a customized gtf comprising the default Ensembl gtf together with annotation for an additional 87 774 lncRNAs that were present in the NONCODEv5 database (http://www.noncode.org/). The mean number of transcriptome-aligned reads per heart, as determined by NONCODEv5, was 5.9×10^5. LncRNAs, identified by NONCODEv5, were defined at a detectable cutoff of 6 reads in at least 50% of the samples in either group, resulting in 15 695 lncRNAs. Fold-change and false discovery rate of the differentially expressed lncRNAs were calculated using the R/Bioconductor packages edgeR and limma/variance modeling at the observational level.

Pathway Analysis

Gene set enrichment analysis (GSEA) was performed on normalized gene counts of DEGs in knockout as compared with control samples ($q<0.05$). Significance was assessed by analyzing signal-to-noise ratio and gene permutations based on 1000 permutations.

Molecular signature database 3.0 curated gene sets for hallmark and canonical pathways were used in the GSEA.[29,30] Gene sets were also curated using the compute overlap, which is a hypergeometric distribution function of GSEA. The data were ordered based on enrichment score for gene set with afalse discovery rate cutoff of 0.05. When presenting results for specific gene sets, nominal enrichment score and false discovery rate values are shown.

Upstream Regulators Analysis

To identify likely TRs, the Upstream Regulator Analysis module of Ingenuity Pathway Analysis software (IPA, QIAGEN, Redwood City, CA) was used. DEGs ($q<0.05$) were used for this analysis. A Z score $\geq+2$ and ≤-2 was used to identify upstream regulators that were predicted to be altered and considered significantly changed. Targets of upstream regulators that overlap with DEGs and show expression pattern consistent with upstream regulator activation or suppression were obtained from IPA.

LncRNA-mRNA Correlation Analysis

Correlation between LncRNA and mRNAs was performed on the count-per-million values for each lncRNA and mRNA in all samples using Pearson correlation analysis in R. Cis pairs for lncRNAs and mRNAs (located within 10 kb) were obtained using the "Nearest BEDTOOL" in local galaxy server platform (https://usegalaxy.org/). Heat plot and density plots that used the Pearson correlation coefficient r values were plotted in R.

Transduction of Mouse Heart With Recombinant AAV9 Constructs

Full-length WT and N-terminally Flag-tagged murine *Lmna* cDNAs were cloned into a pTRUF11 plasmid downstream to a TATA-less CMV promoter and rabbit beta-globin intron at the StuI cloning site and were tested (Figure S1A through S1C). Expressions of the full-length Flag-tagged and nontagged LMNA proteins from the corresponding clones were analyzed by western blotting after transfection of the recombinant plasmids into HEK293 cells using transfectamine (Figure S1B). Approximately 1×10^{10} to 2×10^{10} vector genomes were injected subcutaneously at the nape of the back of *Lmna*$^{-/-}$ mice (*Lmna*$^{-/-}$:AAV9-*Lmna*^{WT}) at postnatal days 2, 4, and 6. The early timing of injection was chosen to ensure adequate gene expression before the *Lmna*$^{-/-}$ mice exhibit cardiac dysfunction enabling an unconfounded transcriptomic analysis.[17] Three sequential injections were made to increase the likelihood of transducing newly formed cardiac myocytes during the early postnatal period, as a low level of proliferation continues this period.[31–33] As a control, an empty AAV9 vector construct was injected into *Lmna*$^{-/-}$ mice at the above time points and via the same subcutaneous route.

AAV9 Transduction Efficiency in Heart and Cardiac Myocytes

Transduction efficiency of the FLAG-LMNA was determined at 1, 2, and 4 weeks after transduction. At least 2000 DAPI-stained cells per each mouse heart were counted. Transduction efficiency was calculated as the percentage of FLAG-stained cells to the total number of cells, identified by DAPI staining of the nuclei, assuming that one third of the DAPI-stained cells in the heart were cardiac myocytes and that only myocytes are transduced with the AAV9 recombinant viruses in the heart.

To determine efficiency following transduction with the recombinant viruses expressing WT LMNA in the *Lmna*$^{-/-}$ mouse hearts, optimal cutting temperature–fixed thin myocardial cryosections were stained with an antibody against PCM1, and an antibody against LMNA and DAPI (nuclei).[31–33] The number of PCMI1 and LMNA costained cells (ie, myocytes) expressing LMNA was determined to confirm transduction efficiency of cardiac myocytes in the mouse heart. Data were analyzed without prior knowledge of the genotypes.

Statistical Analysis

Normality of data distribution was assessed by the Shapiro–Wilk test. Normally distributed data were analyzed by ordinary 1-way ANOVA followed by Tukey's multiple pairwise comparison test. Data deviating from normal distribution were analyzed by the Kruskal–Wallis test followed by Dunn's multiple pairwise comparisons. The categorical data were analyzed by chi-square test. The effect of AAV9-*Lmna*^{WT} on overall survival was evaluated by the Kaplan–Meier survival analysis, and the differences between subgroups were evaluated by log-rank (Mantel-Cox) test. Statistical analysis was performed by GraphPad Prism 8 (www.graphpad.com/scientific-software/prism/).

Data Access

The *Lmna*$^{-/-}$ and WT heart RNA seq data have been submitted to NCBI GEO and are publicly available (GSE110341 and GSE123916). RNA seq data from the *Lmna*$^{-/-}$:AAV9-*Lmna*^{WT} and the corresponding *Lmna*$^{-/-}$ have been submitted to GEO (GSE135288, reviewer token: gxylyyswhxopbsp) and will be released to the public upon manuscript publication.

RESULTS

Phenotype in the *Lmna*$^{-/-}$ Mice

The *Lmna*$^{-/-}$ mice develop progressive cardiac dilatation and dysfunction starting after 2 weeks of age, leading to premature death by 8 to 10 weeks of age.[17] Myocardial histopathology at 3 to 4 weeks of age is notable for increased fibrosis and apoptosis. The *Lmna*$^{-/-}$ mice have a median survival of 4 weeks, as described previously.[17]

AAV9-Mediated Reexpression of WT LMNA (LMNA^{WT}) in *Lmna*$^{-/-}$ Mouse Hearts

To determine the role of LMNA in regulation of cardiac gene expression, we compared gene expression upon loss of LMNA (*Lmna*$^{-/-}$ or KO mice) and upon reexpression of LMNA in the LMNA null background (*Lmna*$^{-/-}$:AAV9-*Lmna*^{WT} mice). A prerequisite to this approach is the ability to effectively express LMNA and to detect its expression and localization in the heart. Therefore, initial experiments were performed using recombinant AAV9 viruses expressing a FLAG-tagged LMNA, which enabled detection of the transgene protein while avoiding the confounding effect of any potential residual expression of the endogenous LMNA protein in the heart of the *Lmna*$^{-/-}$ mice. Two factors were considered in determining timing of administration of the AAV9 viruses: (1) the short life span of the *Lmna*$^{-/-}$ mice, which was at most 8 to 10 weeks; and (2) a short delay in gene expression upon transduction with the AAV9 viruses. Therefore, in vivo gene transfer with the recombinant viruses started at postnatal day 2. To overcome the potential episomal loss of the viral genome caused by actively dividing myocytes during the few days after birth, injections were repeated at postnatal day 4 and postnatal day 6. A total dose of 2×10^{10} viral genome particle was delivered subcutaneously to each neonate.

To detect expression of the transgene in the hearts of *Lmna*$^{-/-}$:AAV9-*Lmna*^{Flag} mice, thin myocardial sections were stained with an anti-FLAG antibody at 1, 2, and 4 weeks after birth, which showed transgene protein expression and nuclear membrane localization in the heart (Figure 1A). Recombinant LMNA protein level was the lowest and regional heterogeneity was more prominent at 1 week after injection, while transgene expression was mostly homogenous and robust at 2 and 4 weeks following transduction with AAV9-*Lmna*^{Flag}. Approximately 19.3±3.2 % of the nuclei showed expression of the FLAG-tagged LMNA, which corresponds to transduction of approximately 57% of myocytes (Figure 1B), assuming that about one third of the cells in the heart are cardiac myocytes and that AAV9 primarily transduces myocytes.[34–36]

Having established the feasibility of the approach, the experiments were repeated with an untagged LMNA, to eliminate potential confounding effects that might result from the Flag-tagged LMNA. The *Lmna*$^{-/-}$ mice were injected subcutaneously with recombinant AAV9 viruses expressing nontagged LMNA^{WT} (*Lmna*$^{-/-}$:AAV9-*Lmna*^{WT}) protein, as described above. Thin myocardial sections obtained from 2-week-old *Lmna*$^{-/-}$ mice were stained with antibodies against LMNA and PCM1, the latter marking cardiac myocyte nuclei. The PCM1 along with LMNA staining of cardiac myocyte was used as a surrogate to determine the transduction and provide a quantitative measure of the overall experimental efficiency. The PCM1-stained cells comprised approximately 35% of the nuclei in the myocardial sections, which is consistent with the previous data.[31–33] There were no differences in the percent PCM1-positive nuclei among the experimental groups. At a dose of 2×10^{10} viral genome particle, 42±6.24% of cardiac myocytes, identified by PCM1 expression, were transduced and expressed LMNA^{WT}, which was incorporated into the nuclear membrane (Figure 1C and 1D). Furthermore, the expression of LMNA protein in the hearts of the AAV9 treated *Lmna*$^{-/-}$ mice was confirmed by immunoblot analysis using an antibody that detects either LMNA or lamin A/C (Figure 1E). A degree of variability in the expression of LMNA was noted in the rescued group (Figure 1F).

Effects of LMNA on Expression of Coding Genes in the Heart

To identify *Lmna* regulated genes, RNA sequencing was performed from 2-week old WT, *Lmna*$^{-/-}$ and *Lmna*$^{-/-}$:AAV9-*Lmna*^{WT} mouse hearts. At 2 weeks of age, there was no discernible cardiac dysfunction or myocardial fibrosis (Table S3), as also reported previously.[17] Analysis of the cardiac gene expression showed differential expression of 2036 genes, comprised of 814 upregulated and 1222 downregulated genes ($q<0.05$) in the *Lmna*$^{-/-}$ as compared with WT mouse hearts (Figure 2A).

Reexpression of LMNA led to the complete or partial reversal of a large fraction of the DEGs. Changes in the expression of the genes upon AAV9 administration were defined as follows:

1. Completely rescued genes: Genes whose expression levels were changed in the *Lmna*$^{-/-}$ hearts but were normalized upon AAV9-*Lmna*^{WT} injection. These genes were considered completely rescued and likely bonafide LMNA regulated genes. Accordingly, transcript levels of these genes were significantly different ($q<0.05$) between the *Lmna*$^{-/-}$ and WT mice but were not significantly different ($q\geq0.05$) between the *Lmna*$^{-/-}$:AAV9-*Lmna*^{WT} and

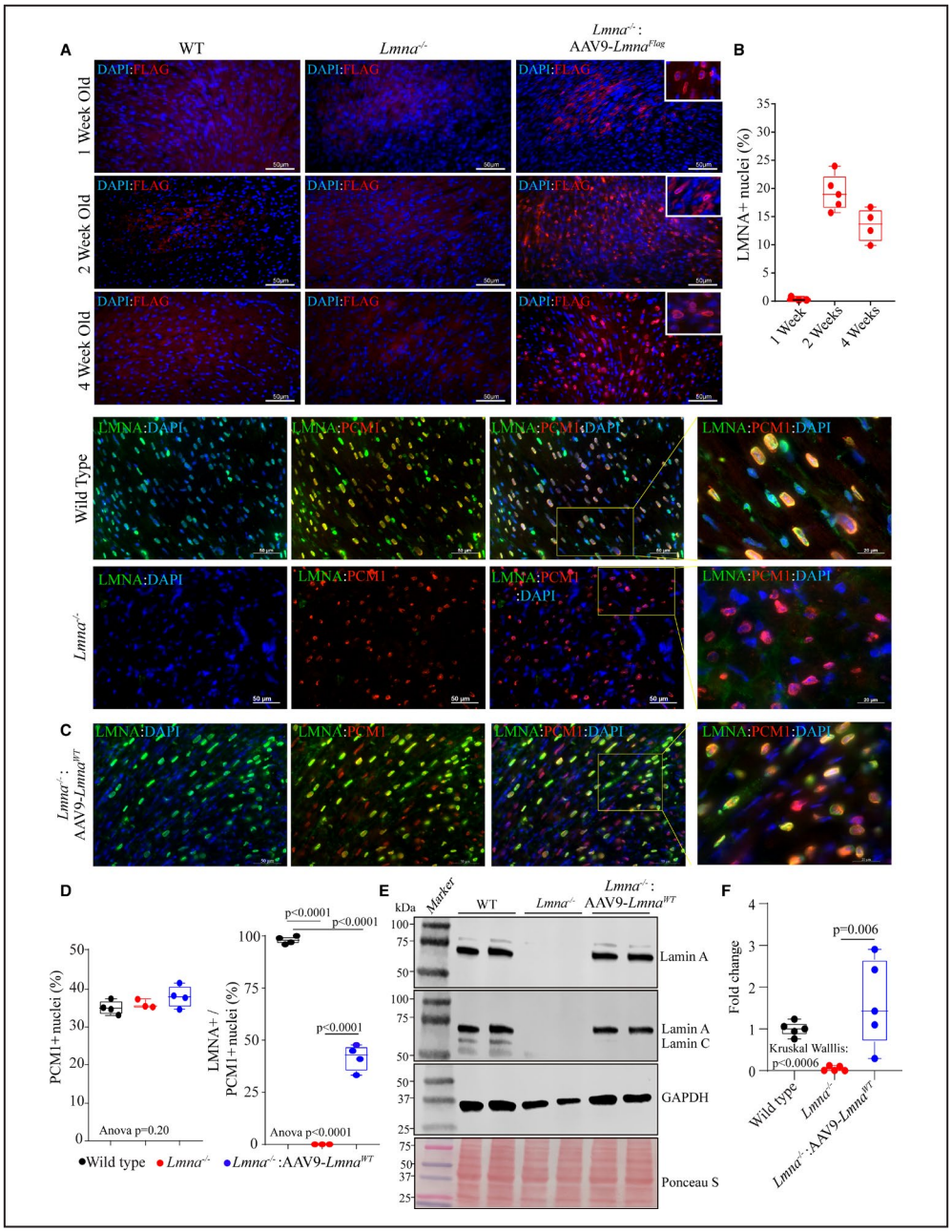

Figure 1. Expression and localization of LMNA in the heart of *Lmna*$^{-/-}$ mice upon AAV9-mediated LMNA re-expression.

A, Immunofluorescence staining of thin myocardial sections showing FLAG-LMNA (in red) expression in 1, 2, and 4-weeks old wild type, *Lmna*$^{-/-}$ and *Lmna*$^{-/-}$:AAV9–*Lmna*^{Flag} mice. Nuclei were counterstained with DAPI (blue). **B**, Respective quantitation of LMNA^{+} nuclei as a fraction of total DAPI^{+} nuclei per heart (n=3–5). **C**, IF staining of myocardial sections in 2 weeks old wild type, *Lmna*$^{-/-}$ and *Lmna*$^{-/-}$: AAV9-*Lmna*^{WT} LMNA (in green) and anti-PCM1 antibody (in red). Higher magnification of the overlay of LMNA and PCM1 with DAPI. **D**, Respective quantitative data showing the percentage of PCM1 positive nuclei (marking cardiac myocytes) in the WT (n=4), *Lmna*$^{-/-}$ (n=3) and *Lmna*$^{-/-}$:AAV9-*Lmna*^{WT} (n=4) and percentage of cardiac myocytes expressing LMNA (PCM1+/LMNA+nuclei). **E**, Immunoblot (IB) showing the expression of LMNA in whole heart lysates of 2-week old mice in WT, *Lmna*$^{-/-}$ and *Lmna*$^{-/-}$:AAV9-*Lmna*^{WT} mice using an anti-LMNA antibody. Protein molecular weight markers are shown to the left, and GAPDH is used as a loading control together with total protein staining using Ponceau S. **F**, Quantitative data for LMNA protein expression fold change normalized to GAPDH and relative to WT mice. Data were obtained from N=5 mice heart/genotype and shows variability in the LMNA protein expression in the AAV9-LMNA treated samples. Normality of data distribution was assessed by Shapiro–Wilks test. *P* values for Kruskal–Wallis test and Dunn's multiple comparison are shown. Only *P* values that were significant ($P<0.05$) are shown. AAV9 indicates adeno-associated virus serotype 9; DAPI, 4′,6-diamidino-2-phenylindole; LMNA, lamin A; PCM1, pericentriolar material-1; and WT, wild-type.

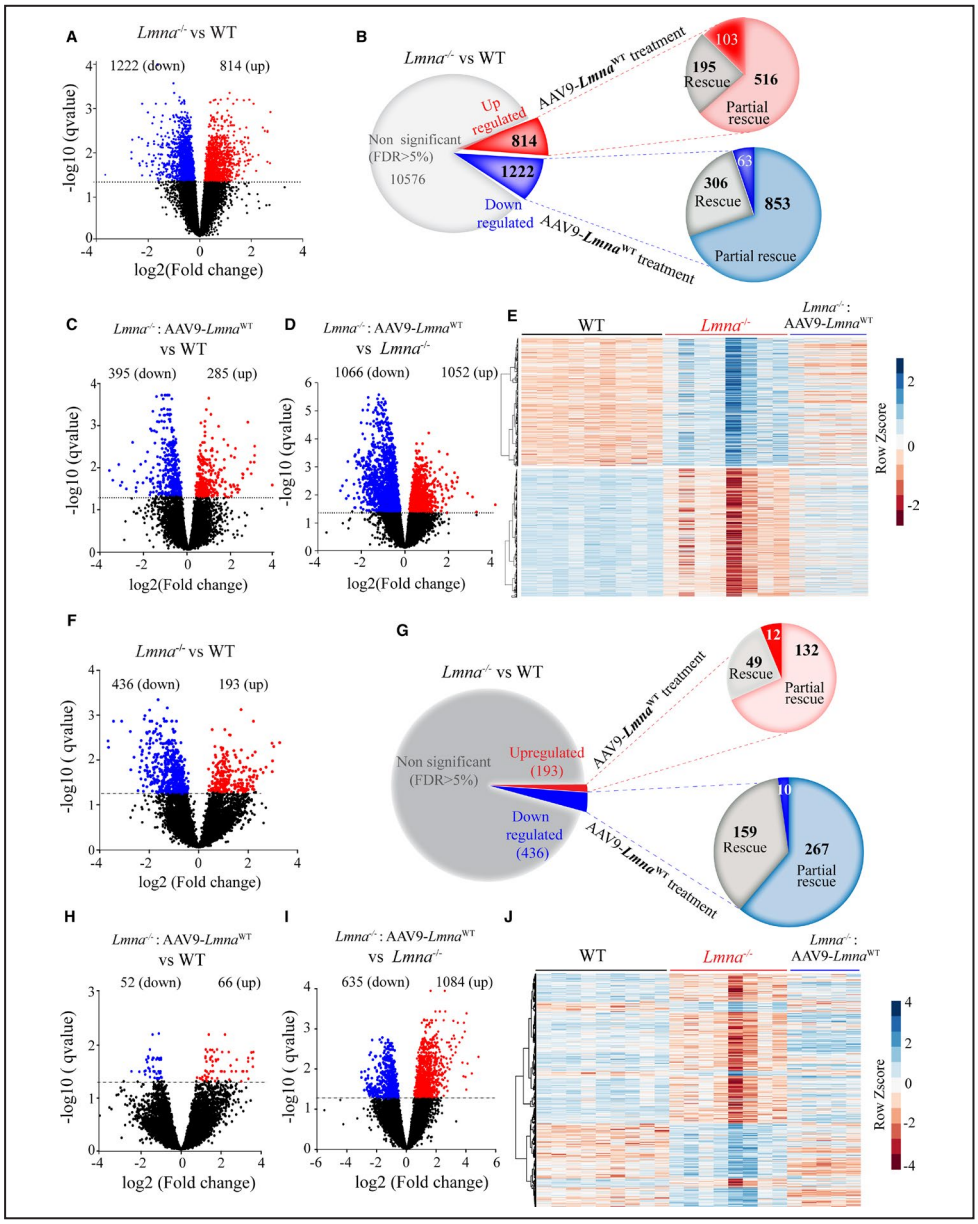

Figure 2. Differential coding and noncoding RNA expression in the WT, *Lmna*$^{-/-}$ and *Lmna*$^{-/-}$: AAV9-*Lmna*^{WT} mouse hearts at 2 weeks of age.

A, Volcano plots of RNA sequencing data showing the expression and significance levels of genes in *Lmna*$^{-/-}$ (n=8) vs WT (n=9) hearts. The dashed line denotes the significance level at a threshold of q<0.05 (or false discovery rate 5%). The up-regulated and (are red), down regulated genes (blue) are shown. Number of upregulated and down regulated differentially expressed genes (DEGs) are indicated above each volcano plots. **B**, Pie charts illustrating the number of differentially upregulated (red), downregulated (blue), and unchanged (gray) genes in *Lmna*$^{-/-}$ hearts compared with the WT (q<0.05). A subset of genes that show complete and partial rescue upon AAV9 treatment (n=5) are shown along with the unaffected ones. **C** and **D**, Volcano plots of RNA-seq data showing the expression and significance levels of genes in the *Lmna*$^{-/-}$:AAV9-*Lmna*^{WT} vs *Lmna*$^{-/-}$ (**C**) and *Lmna*$^{-/-}$:AAV9-*Lmna*^{WT} vs WT (**D**) heart. **E**, Heat map and hierarchical clustering of differentially expressed genes in the *Lmna*$^{-/-}$ compared with WT mouse hearts and the corresponding expression upon LMNA expression (*Lmna*$^{-/-}$:AAV9-*Lmna*^{WT}). **F**, Volcano plots of the RNA sequencing data showing the expression and significance levels for lncRNAs in the *Lmna*$^{-/-}$ vs WT hearts. **G**, Pie charts illustrating the number of differentially upregulated (red), downregulated (blue), and unchanged (gray) lncRNAs in *Lmna*$^{-/-}$ hearts compared with the WT (q<0.05). A subset of lncRNAs that show complete and partial rescue upon AAV9 treatment are shown along with the ones that are unaffected. **H** and **I**, Volcano plots for lncRNA expression in the *Lmna*$^{-/-}$: AAV9-*Lmna*^{WT} vs *Lmna*$^{-/-}$ (**H**) and in the *Lmna*$^{-/-}$:AAV9-*Lmna*$^{WT-}$ vs WT (**I**) mouse hearts. **J**, Heat map with hierarchical clustering of differentially expressed lncRNAs in *Lmna*$^{-/-}$ compared with WT mouse hearts and corresponding changes upon LMNA expression in the *Lmna*$^{-/-}$ mouse hearts. AAV9 indicates adeno-associated virus serotype 9; LMNA, lamin A; lncRNA, long noncoding RNA; and WT, wild-type.

WT groups. Therefore, transcript levels of these genes were considered normalized. The completely rescued genes comprised 23.9% of the upregulated (195/814) and 25.1% (306/1222) of the downregulated genes in the *Lmna*$^{-/-}$ hearts (Figure 2B and Figure S2A).

2. Partially rescued genes: Dysregulated genes in the *Lmna*$^{-/-}$ heart whose expression levels were significantly improved upon administration of the *Lmna*$^{-/-}$:AAV9-*Lmna*^{WT} ($q<0.05$ as compared with their levels in the *Lmna*$^{-/-}$ hearts) but were not completely restored to normal levels and were not significantly different from the levels in the WT hearts. The majority of the DEGs were in this category, which included 63.3 % of the upregulated (516/814) and 69.8% of the downregulated (853/1222) genes (Figure 2B and Figure S2B).
3. Unchanged genes: Genes whose expression levels did not change upon injection of the AAV9-*Lmna*^{WT} viruses in the *Lmna*$^{-/-}$ hearts. Therefore, transcript levels of these genes remained altered in the *Lmna*$^{-/-}$: AAV9-*Lmna*^{WT} hearts as compared with WT hearts. Thus, the reexpression of the LMNA did not affect the expression levels of this set of genes. This group of genes comprised 12.60% (103/814) of the upregulated and 5% (63/1222) of downregulated genes (Figure 2B and Figure S2C).

Thus, considering the above, cardiac gene expression profile in the *Lmna*$^{-/-}$: AAV9-*Lmna*^{WT} mice closely resembled that of the WT mice, as only 680 genes remained differentially expressed between these 2 groups (Figure 2C). Compared with the *Lmna*$^{-/-}$ mice, the reintroduction of LMNA in the heart was associated with increased expression levels of 1052 genes and suppressed expression levels of 1066 genes (Figure 2D). Hierarchical clustering of DEGs showed that cardiac transcriptomic profile in the *Lmna*$^{-/-}$: AAV9-*Lmna*^{WT} mice was closer to that in WT mice but was distinct from the transcript profile in *Lmna*$^{-/-}$ mouse hearts (Figure 2E).

Effects of LMNA on the Expression of Noncoding RNA Expression in the Heart

We have shown before that LADs were predominantly enriched at the noncoding and heterochromatic regions in human cardiac myocytes.[13] Therefore, effects of LMNA deficiency and reexpression on noncoding RNAs were analyzed. The noncoding RNAs (henceforth lncRNA), antisense RNAs, sense overlapping, and divergent transcripts, were included in the analysis, whereas snoRNAs, pre-miRNA, and pseudogenes were excluded. A total of 629 lncRNAs were differentially expressed (193 upregulated and 436 downregulated) in *Lmna*$^{-/-}$ compared with WT mouse hearts (Figure 2F). Reexpression of LMNA in the heart completely rescued 49 of 193 (25.4%) of the upregulated and 159 of 436 (36.5%) of the downregulated lncRNAs in the heart (Figure 2G). The corresponding numbers for partial rescue were 132 of 193 (68.4%) for upregulated and 267 of 436 (61.2%) for downregulated lncRNAs (Figure 2G). In contrast, expression levels of only 118 lncRNAs were significantly different between the *Lmna*$^{-/-}$: AAV9-*Lmna*^{WT} and WT groups (Figure 2H). Finally, as compared with *Lmna*$^{-/-}$ mouse heart, 1698 lncRNA were differentially expressed in the *Lmna*$^{-/-}$: AAV9-*Lmna*^{WT} (Figure 2I). Consequently, hierarchical clustering analysis of the lncRNAs showed the *Lmna*$^{-/-}$: AAV9-*Lmna*^{WT} group was clustering with the WT as compared with *Lmna*$^{-/-}$ mice (Figure 2J).

Effects of LMNA on Dysregulated Regulatory Network and Biological Pathways

GSEA was performed to identify biological pathways regulated by LMNA. Only genes that were classified as completely rescued were used for this analysis (Figure 3A). GSEA using the Hallmark Molecular Signature showed restoration of LMNA regulated pathways that are mainly involved in inflammation, cell death, and fibrosis through tumor necrosis factor-α signaling, TP53 (tumor protein 53) and epithelial to mesenchymal transition. The pathways were predicted to be upregulated in the *Lmna*$^{-/-}$ compared with WT mouse hearts (Figure 3B) and suppressed in the *Lmna*$^{-/-}$: AAV9-*Lmna*^{WT} as compared with *Lmna*$^{-/-}$ mouse hearts. Likewise, among the suppressed pathways genes involved in oxidative phosphorylation, E2F pathway, and G2M checkpoint (Figure 3C) were rescued as shown by suppression of these pathways in *Lmna*$^{-/-}$ (compared with WT) and reversal upon reexpression of LMNA in the heart (*Lmna*$^{-/-}$: AAV9-*Lmna*^{WT} compared with *Lmna*$^{-/-}$, Figure 3C).

However, several pathways did not show rescue upon *Lmna*$^{-/-}$: AAV9-*Lmna*^{WT} treatment (Table S4). Noteworthy among them was the gene set for apoptosis that showed induction in *Lmna*$^{-/-}$ versus WT group ($q=0.013$, Table S4) but remained unchanged upon AAV9-*Lmna*^{WT} treatment ($q=0.8$, Table S4).

IPA was performed to identify activated (Z score ≥2.0) and suppressed (Z score ≤2.0) biological pathways, as predicted from the DEGs among the 3 groups used as input (Figure 3D). IPA identified a subset of pathways and thereby reversal of Z score values upon AAV9-*Lmna*^{WT} treatment (Figure 3E). Likewise, some pathways showed only incomplete reversal of gene signature (Figure 3F) and their Z score was closer to WT upon AAV9-*Lmna* treatment and did not reach the threshold cutoff (activated [Z score ≥2.0] and suppressed [Z score ≤−2.0]). Finally, the pathways that were not affected

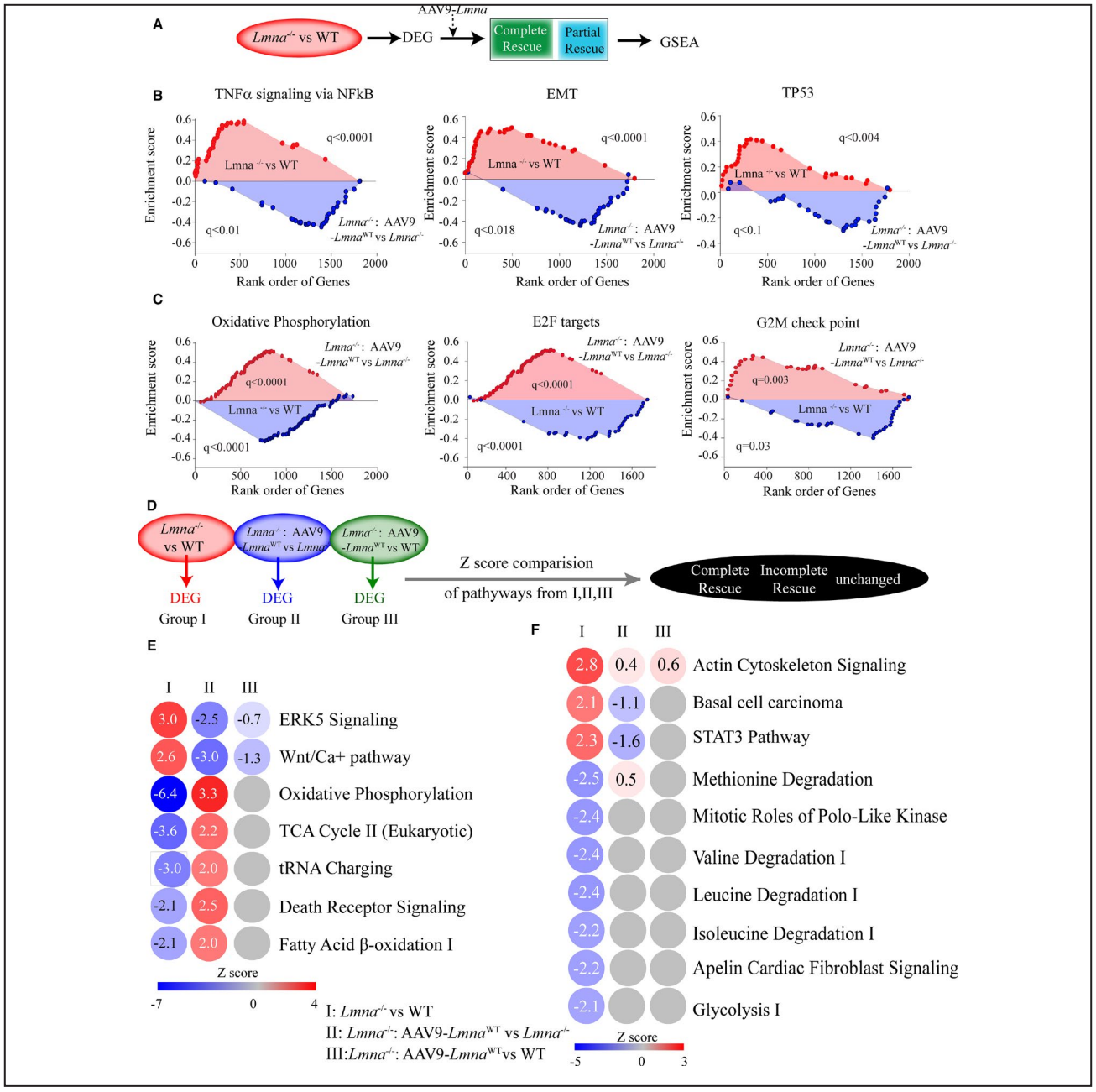

Figure 3. Biological pathways in *Lmna*$^{-/-}$ and upon *Lmna* re-expression.

A, Schematic showing the genes selection for Gene Set Enrichment Analysis (GSEA). **B** and **C**, Top Hallmark signature upregulated (**B**) and downregulated (**C**) in *Lmna*$^{-/-}$ vs WT are shown and their corresponding status upon AAV9-*Lmna*^{WT} treatment (*Lmna*$^{-/-}$:AAV9-*Lmna*^{WT}). **D**, Schematic showing the genes used for Ingenuity Pathway Analysis (IPA). Differentially expressed genes were obtained from *Lmna*$^{-/-}$ vs WT, *Lmna*$^{-/-}$:AAV9-*Lmna*^{WT} vs *Lmna*$^{-/-}$, and *Lmna*$^{-/-}$:AAV9-*Lmna*^{WT} vs WT comparison and used to identify significantly altered pathways. Comparisons of pathways that significantly change in the *Lmna*$^{-/-}$ vs WT (*Z* score ≥2 and ≤−2 and $P<0.05$) were made to those in other groups. **E** and **F**, IPA analysis for enriched pathways comparisons in all three groups. *Z* scores are indicated for each pathway, activated pathways (red), and the inhibited (blue) are shown and the color of the circles is indexed to the Z score values. The comparison in *Lmna*$^{-/-}$ vs WT (first column), *Lmna*$^{-/-}$:AAV9-*Lmna*^{WT} vs *Lmna*$^{-/-}$ (middle column), and *Lmna*$^{-/-}$:AAV9-*Lmna*^{WT} vs WT (right column) are shown. **E**, Depicts the pathways that showed complete reversal defined as ones that are induced or suppressed in *Lmna*$^{-/-}$ vs WT group (Z-score greater than or equal to 2 and less than or equal to −2 and $P<0.05$) and their reversal in *Lmna*$^{-/-}$:AAV9-*Lmna*^{WT} group (*Z* score ≥2 and ≤−2 and $P<0.05$) and no change in *Lmna*$^{-/-}$:AAV9-*Lmna*^{WT} vs WT group. **F**, Partially rescued pathways defined as ones that are induced or suppressed in *Lmna*$^{-/-}$ vs WT group but is not different in the *Lmna*$^{-/-}$:AAV9-*Lmna*^{WT} vs *Lmna*$^{-/-}$ and *Lmna*$^{-/-}$ vs WT group. *Z* score was obtained from IPA. AAV9 indicates adeno-associated virus serotype 9; DEG, differentially expressed gene; EMT, epithelial to mesenchymal transition; ERK5, extracellular signal-regulated kinase 5; GSEA, gene set enrichment analysis; NFκB, nuclear factor kappa-light-chain enhancer of activated B cells; STAT3, signal transducer and activator of transcription 3; TCA, tricarboxylic acid; TNFα, tumor necrosis factor-α; TP53, tumor protein 53; and WT, wild-type.

upon AAV9 treatment showed *Z* score value similar to the *Lmna*$^{-/-}$ group and were characterized as unchanged. Notable were those involved in cardiac hypertrophy/function (extracellular signal-regulated kinase 5 and Wnt), as indicated by their induction (*Z* score ≥2.0) in the *Lmna*$^{-/-}$ mouse hearts and their reversal upon AAV9-mediated LMNA expression (*Z* score ≤–2.0) and thereby, normalization toward WT (Figure 3E). Likewise, pathways involved in cardiac metabolism, mainly in mitochondrial function (oxidative phosphorylation, glycolysis, and fatty acid β-oxidation I), were suppressed in the *Lmna*$^{-/-}$ mouse hearts (Figure 3E) and restored upon LMNA reexpression in *Lmna*$^{-/-}$ mouse hearts (Figure 3D and 3E). Taken together, these findings identify LMNA-regulated pathways and implicate the role for LMNA in cardiac metabolism, cell death, and inflammation.

To identify TRs that were responsible for the dysregulated gene expression and were LMNA dependent, only genes that showed complete rescue and were therefore considered bona fide LMNA-regulated genes were analyzed using the Upstream Regulators Analysis function of IPA. Over a dozen TRs that control this gene dysregulation in *Lmna*$^{-/-}$ were identified, including TP53, KDM5A (as the top candidate TR for activation). Retinoblastoma 1 (RB1) and paired-like homeodomain 2 (PITX2) were identified as most likely TRs to be suppressed in the *Lmna*$^{-/-}$ mouse heart (Table S5).

DEGs were also analyzed to infer the TRs whose activity was restored after reexpression of the LMNA in the heart (Figure 4A). Significantly changed TRs that were identified in each group and then compared with the status of these TRs. According to changes in the DEGs upon administration of the AAV9 viruses, activated TP53, KDM5A, and nuclear receptor–interacting protein 1 were fully rescued, whereas KDM5B, forkhead box O, SMAD3 (Mothers Against Decapentaplegic Homolog 3), and several others were partially rescued (Figure 4B). Similarly, among the suppressed TRs, RB1, PITX2, and melanocyte-inducing transcription factor were completely rescued, and several others were partially rescued (Figure 4C). The complete list of dysregulated TRs and inferred changes in their transcriptional activities upon AAV9 administration are shown in Figure 4B and 4C. A similar analysis of other regulators using IPA for DEG showed rescue of rapamycin-insensitive companion of mTOR, insulin receptor, and serine-threonine kinase 11, and an incomplete rescue of several others (Table S6). Finally, a subset of upstream regulators was inferred as unchanged, including TGF (transforming growth factor-β1) (Table S6), RELA proto-oncogene, NF-kB subunit, signal transducer and activator of transcription 3, CAMP responsive element-binding protein 1 and sex-determining region Y-box 2 (Figure 4D and 4E). Of the upstream TRs identified in this analysis, we have previously implicated TP53 and forkhead box O3 in the pathogenesis of LMNA-associated DCM.[17,19] Notable among the unchanged regulator was TGF, a well-characterized mediator of cardiac fibrosis (see below).

The involvement of KDM5A and B in the laminopathies or cardiac dysfunction were novel findings. Therefore, we curated the KDM5A and B predicted targets from IPA and found that transcript levels of 37 of 42 KDM5A and 15 of 19 KDM5B target genes, were altered in the *Lmna*$^{-/-}$ mouse hearts (Figure 4F). KDM5A targets were enriched for genes involved in mitochondrial biogenesis and function/cardiac energy metabolism (Figure 4G), whereas KDM5B targets showed enrichment of genes involved in cell cycle and cell division (Figure 4H).

To validate activation of the KDM5A in the hearts in the *Lmna*$^{-/-}$ mice, transcript levels of a selected number of KDM5A target genes were analyzed by quantitative polymerase chain reaction, which confirmed decreased transcript levels of KDM5A target genes (Figure 5B). Evaluation of *Kdm5a* and *Kdm5b* mRNAs in these groups did not show any changes in the RNA levels among the experimental groups (Figure 5C). However, immunoblotting performed on myocardial nuclear protein extracts using antibodies that detect KDM5A and B showed increased nuclear levels of KDM5A by 18.3±8.9-fold (n=3; P=0.02) and KDM5B by 7.5±2.7-fold (n=3; P=0.008) in the *Lmna*$^{-/-}$ as compared with WT mouse hearts (Figure 5D). AAV9-mediated LMNA reexpression partially rescued KDM5A and B protein levels in the *Lmna*$^{-/-}$ mouse hearts (Figure 5E). The data provided additional evidence of KDM5 dysregulation in the *Lmna*$^{-/-}$ mouse hearts.

LncRNA, mRNA Coexpression Network

Unlike protein-coding genes, the majority of lncRNAs do not yet have defined biological functions. However, lncRNAs have been observed to regulate expression of mRNAs by acting in cis or trans, which enables the prediction of lncRNAs functions based upon co-regulated mRNAs as proxies.[35,36] Pairwise analysis of completely rescued 207 lncRNA and 501 mRNAs revealed multiple strong correlations for lncRNA: mRNA pair, as indicated by a high *r*-value (Figure S3A). Analysis of partially rescued 399 lncRNAs and 1369 mRNAs also showed a similar pairwise correlation (Figure S3A and S3B). Next, we reasoned that expressions of lncRNAs and mRNAs belonging to the similar biological pathways are likely to be coordinated and, thereby, are expected to show a high correlation in their expression pattern. To ascertain the biological roles of differentially expressed lncRNAs, we obtained highly correlated lncRNA: mRNA

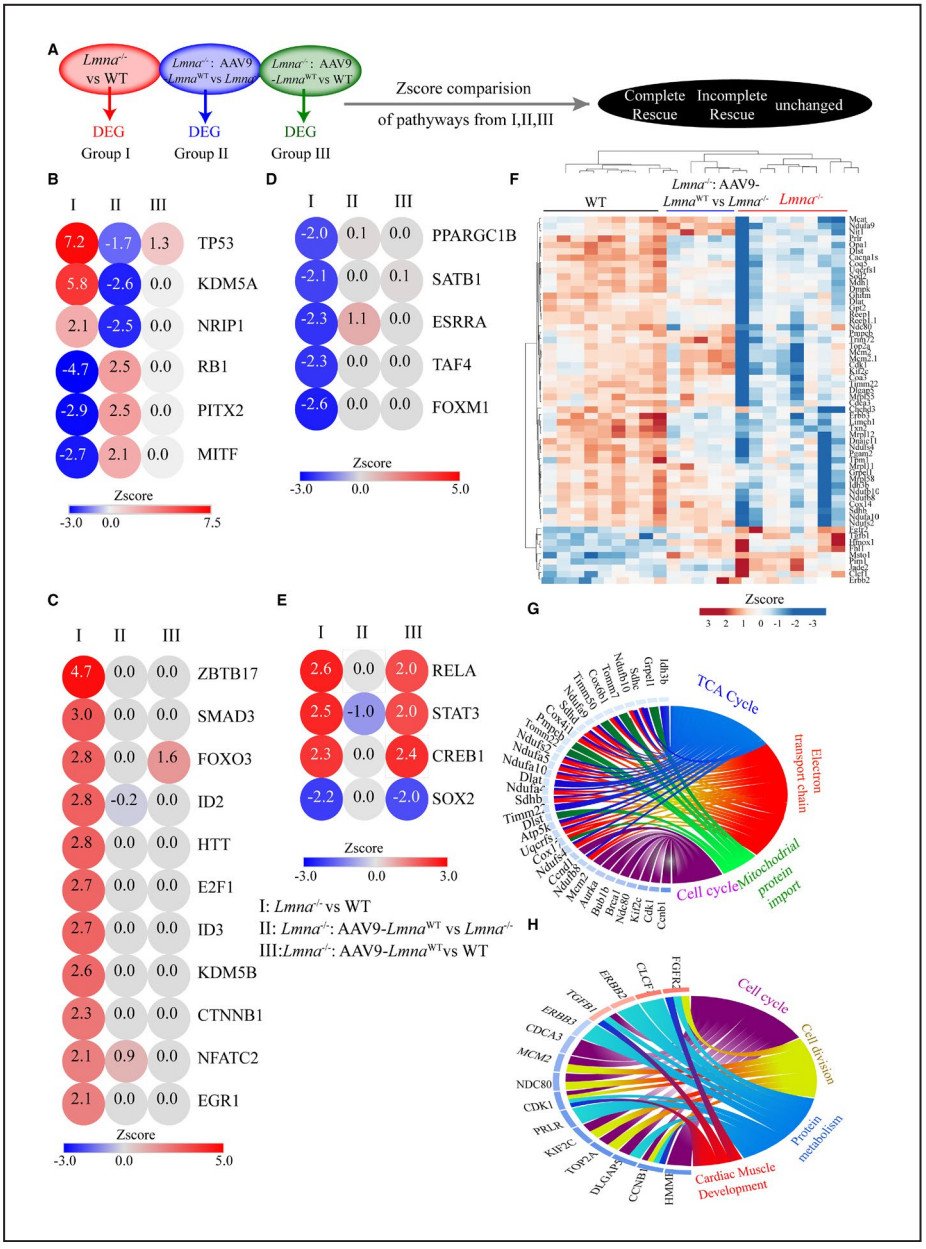

Figure 4. Transcriptional regulators (TR) perturbed in the *Lmna*$^{-/-}$ mice and their rescue in AAV9-*Lmna*^{WT} treated hearts.

A, Schematic showing the genes used for Ingenuity Pathway Analysis (IPA). **B** through **E**, IPA analysis for upstream regulator showing top dysregulated TRs. Z-Score comparisons for indicated TRs in 3 experimental groups are plotted. Activated ones are shown in red, and the inhibited in blue. The color of the circles is indexed to the *Z* score values. The experimental group used for comparison are marked as follows (I) *Lmna*$^{-/-}$ vs WT, (II) *Lmna*$^{-/-}$:AAV9-*Lmna*^{WT} vs *Lmna*$^{-/-}$ (III) *Lmna*$^{-/-}$:AAV9-*Lmna*^{WT} vs WT. **B**, Denotes complete reversal, (**C**) shows incompletely rescued upregulated and (**D**) shows incompletely rescued downregulated TRs. **E**, TR not affected by LMNA reexpression. **F**, Heat plot of the lysine-specific demethylase 5A (KDM5A) and B targets genes that show overlap with the IPA curated database and show expression pattern consistent with KDM5A and B activation. Hierarchical clustering of the genes shows that WT and AAV9-LMNA^{WT} injected *Lmna*$^{-/-}$ cluster together and are distinct from the *Lmna*$^{-/-}$ group. **G** and **H**, Circos plot of gene ontology analysis of KDM5A (**G**) and KDM5B (**H**) targets that are differentially expressed in *Lmna*$^{-/-}$ mouse hearts compared with WT. AAV9 indicates adeno-associated virus serotype 9; LMNA, lamin A; and WT, wild-type.

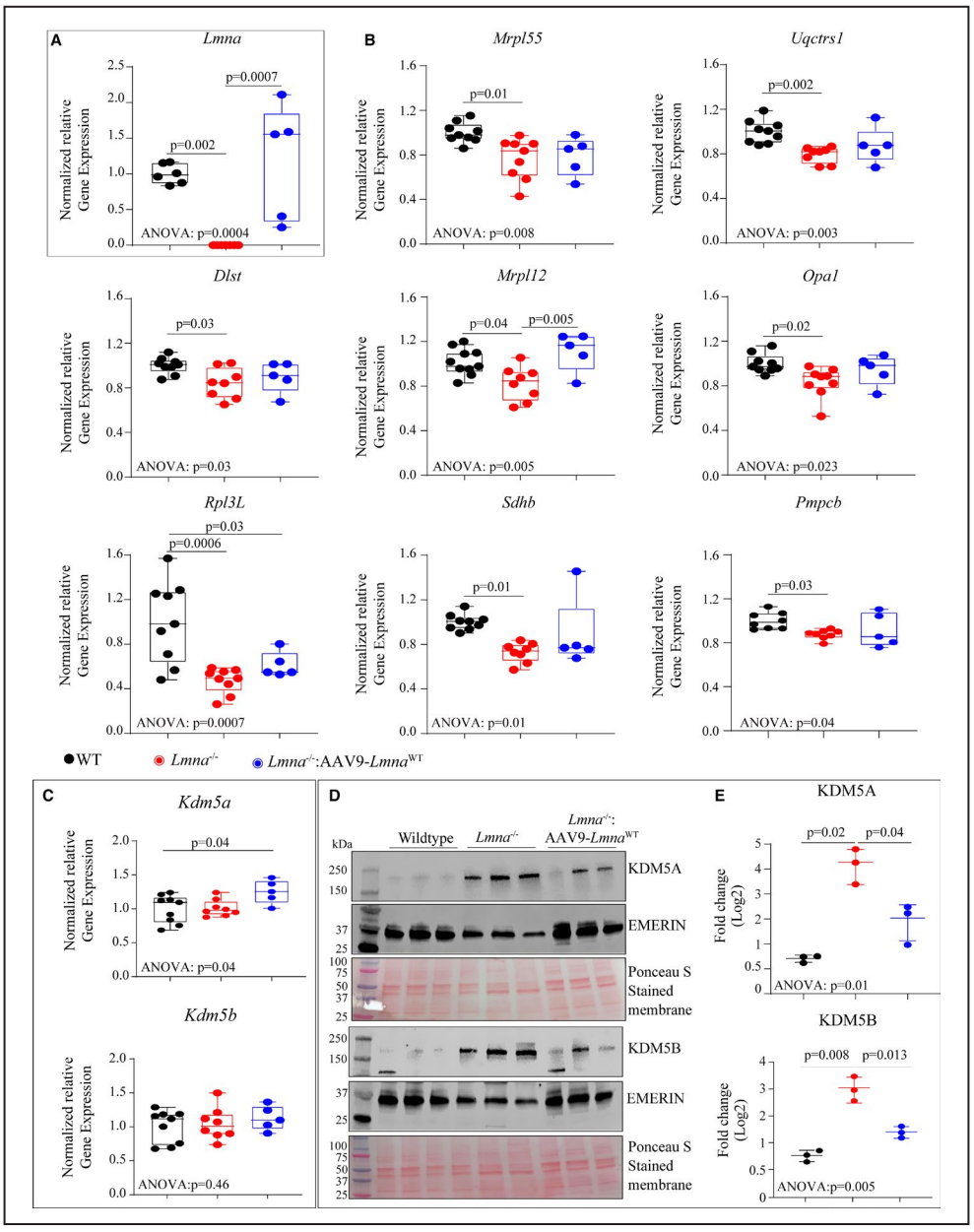

Figure 5. I KDM5A and B are activated in *Lmna*$^{-/-}$ and partially rescued in AAV9-*Lmna*^{WT} treated hearts.

Quantitative PCR (qPCR) analysis of *Lmna* (**A**) and targets of KDM5A and KDM5B (**B**) in the WT, *Lmna*$^{-/-}$ and AAV9-LMNA^{WT} injected mice. **C**, qPCR analysis of *Kdm5a* and *Kdm5b* mRNAs showed no differential expression in the indicated groups. **D**, Immunoblot of nuclear extract from WT, *Lmna*$^{-/-}$ and AAV9-LMNA^{WT} injected *Lmna*$^{-/-}$ mouse hearts showing KDM5A (top panel) and KDM5B (lower panel) using anti-KDM5A and anti-KDM5B antibodies. Emerin was used as a nuclear loading control and Ponceau S stained membranes are shown to assess similar loading patterns. **E**, Respective quantitative data of KDM5A and KDM5B in the nuclear fraction in the heart of WT, *Lmna*$^{-/-}$, and *Lmna*$^{-/-}$: AAV9-LMNA^{WT} mice (n=3). For normally distributed dataset, 1-way ANOVA followed by Tukey's multiple pairwise comparison *P* values are shown and for once not normally distributed Kruskal–Wallis followed by Dunn's multiple pairwise comparison *P*-values are shown. Only *P*-values that were significant ($P<0.05$) are shown. AAV9 indicates adeno-associated virus serotype 9; KMD5, lysine-specific demethylase 5; LMNA, lamin A; and WT, wild-type.

pairs that showed a Pearson correlation coefficient (r) >0.9 or −0.9 (Figure S3C). IPA for biological pathways involving these mRNAs (as a surrogate for the correlated lncRNAs), showed enrichment for genes involved in oxidative phosphorylation (Figure S3D). Further analysis for the transcriptional regulators of

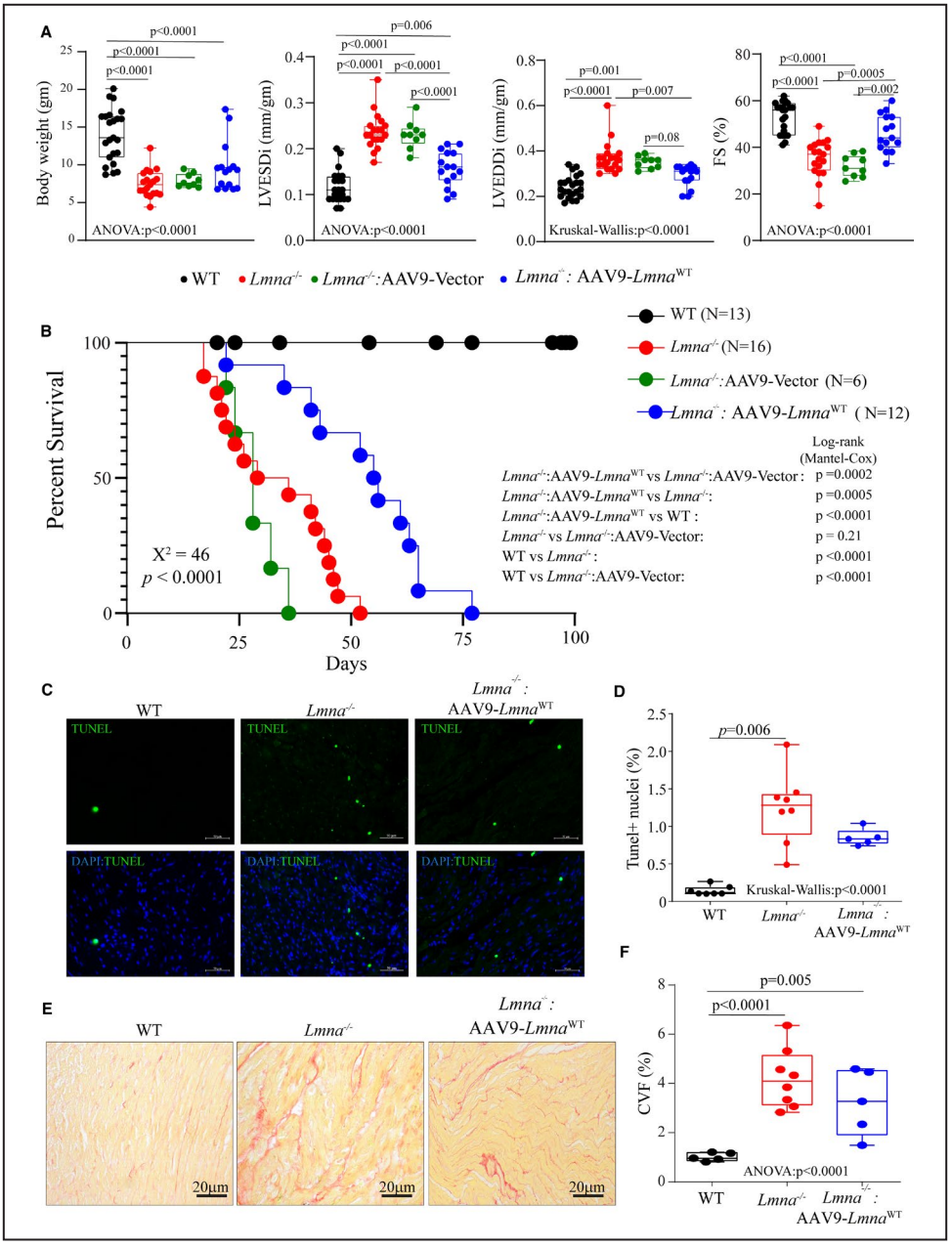

Figure 6. Phenotypic consequences of AAV9 mediated *Lmna*^{WT} expression in the *Lmna*$^{-/-}$ mice. **A**, Selected echocardiographic indices of cardiac structure and function showing improvement of cardiac function upon vector or AAV9-*Lmna*^{WT} injection of *Lmna*$^{-/-}$ mice at 4 weeks after birth. LVEDDi: Left Ventricular End-Diastolic Diameter indexed to the bodyweight; LVESDi, left ventricular end-systolic diameter indexed to the bodyweight; FS, fractional shortening (age, sex, and number of mice used in each group are listed in Tables S3 and S7). **B**, Kaplan–Meier survival plots of WT, *Lmna*$^{-/-}$, and *Lmna*$^{-/-}$ mice injected with vector or AAV9 expressing Lmna^{WT}. Chi-square and *P* value for the overall Kaplan–Meier survival analysis are indicated in bold. Log-rank (Mantel-Cox) pairwise analysis *P* values for each subgroup analysis are shown. **C**, Representative terminal deoxynucleotidyl transferase deoxyuridine triphosphate nick end labeling (TUNEL) stained thin myocardial cross-section from 4-week-old WT, *Lmna*$^{-/-}$, and *Lmna*$^{-/-}$: AAV9-*Lmna*^{WT} are shown. The lower panel shows overlay images of TUNEL staining in green and nuclei (blue). **D**, Respective quantitative data of the TUNEL-positive stained nuclei in WT (n=7), *Lmna*$^{-/-}$ (n=8), and *Lmna*$^{-/-}$ mice injected with AAV9-*Lmna*^{WT} (n=5). **E**, Representative Picrosirius red-stained thin myocardial sections from 4-week-old WT, *Lmna*$^{-/-}$, and *Lmna*$^{-/-}$: AAV9-*Lmna*^{WT}. **F**, Respective quantitative data on collagen volume fraction in WT (n=5), *Lmna*$^{-/-}$ (n=8), and *Lmna*$^{-/-}$ mice injected with AAV9-*Lmna*^{WT} (n=5). One-way ANOVA followed by Tukey's multiple pairwise comparison *P* values is shown. Only *P* values that were significant (*P*<0.05) are shown. AAV9 indicates adeno-associated virus serotype 9; KMD5, lysine-specific demethylase 5; and WT, wild-type.

the correlated mRNAs showed enrichment for targets of TP53, KDM5A, NUPR1, predicting their activation in the *Lmna*$^{-/-}$ mouse hearts. In contrast, transcriptional regulators RB1, peroxisome proliferator–activated receptor gamma coactivator 1-α, peroxisome proliferator–activated receptor gamma coactivator 1-β, and PITX2 were predicted to be suppressed (Figure S3E and S3F).

Phenotypic Consequences of Reexpression of LMNA^{WT} in *Lmna*$^{-/-}$ Mouse Hearts

The *Lmna*$^{-/-}$ mice exhibited cardiac dilatation and dysfunction at 4 weeks of age in accordance with previously published data, as indicated by a marked increase in left ventricular end-diastolic and systolic diameters, and reduced left ventricular fractional shortening (Table S7). Consistent with the partial rescue of differentially expressed coding and noncoding genes, AAV9 mediated reexpression of LMNA^{WT} improved cardiac function in the *Lmna*$^{-/-}$ mice, as noted by improvement in the echocardiographic indices of cardiac size (left ventricular end-diastolic diameter and left ventricular end-systolic diameter, Figure 6A) and function (Figure 6A and Tables S3 and S7). The improvement in cardiac function was associated with prolonged median survival (Figure 6B), from 28 days in the *Lmna*$^{-/-}$ mice to 52 days in the *Lmna*$^{-/-}$:AAV9*Lmna*^{WT} mice. Treatment of *Lmna*$^{-/-}$ mice with control viruses comprised of the AAV9 viral genome but without the *Lmna* gene did not affect survival (Figure 6B and Figure S4) or cardiac function (Figure 6A and Table S7). Likewise, treatment of *Lmna*$^{-/-}$:AAV9*Lmna*^{Flag} had a similar improvement in survival and cardiac function (Figure S4 and Table S8), further indicating that the FLAG epitope did not interfere with the beneficial effect of *Lmna* reexpression.

Given that myocardial apoptosis is a phenotypic feature of the *Lmna*$^{-/-}$ mice and in view of activation of TP53 pathway,[19] the effect of reexpression of LMNA on cell death was evaluated by terminal deoxynucleotidyl transferase deoxyuridine triphosphate nick end labeling TUNEL assay in heart sections. Consistent with the previous data,[17] the *Lmna*$^{-/-}$ mice showed increased TUNEL positive cells (1.24±0.47% in *Lmna*$^{-/-}$ versus 0.14±0.06% in WT control mice, $P<0.001$). Upon AAV9 treatment the number of TUNEL positive cells showed a trend toward a reduction in the *Lmna*$^{-/-}$:AAV9*Lmna*^{WT} hearts (0.85±0.11% in AAV9-treated versus 1.24±0.47% in *Lmna*$^{-/-}$ mice, $P=0.09$, Figure 6C and 6D). Gene expression analysis of cell death genes with quantitative polymerase chain reaction also showed a similar trend with partial or no rescue upon AAV9 treatment (Figure S5A). Myocardial fibrosis quantitated and represented as collagen volume fraction was increased in *Lmna*$^{-/-}$ mice (3.59±1.32% in *Lmna*$^{-/-}$ versus 1.02±0.15% in WT, $P=0.0003$). However, the re-expression of the LMNA^{WT} did not have a discernible effect on collagen volume fraction in the *Lmna*$^{-/-}$ mice (3.23±1.34% in *Lmna*$^{-/-}$: AAV9-*Lmna*^{WT} versus 3.59±1.32% in *Lmna*$^{-/-}$, $P=0.9$, Figure 6E and 6F). Consistent with this observation AAV9-*Lmna*^{WT} treatment did not rescue the molecular signature of cardiac fibrosis, as indicated by the unchanged status of TGF, a key regulator of fibrosis in the treated group (Table S6). Likewise, quantitative polymerase chain reaction analysis of selected fibrosis markers showed partial or no rescue in the treated group (Figure S5B).

DISCUSSION

LMNA, a ubiquitously expressed protein in differentiated cells, interacts with numerous genomic regions through LADs, and influences chromatin structure.[12,13,17,37,38] We determined early transcriptomic changes (before the onset of cardiac dysfunction) in the hearts of *Lmna*$^{-/-}$ mice, compared with WT mice and following reexpression of LMNA in the *Lmna*$^{-/-}$ mouse heart. The approach was taken to reduce potential confounding effects of cardiac dysfunction on gene expression and identify DEGs and pathways that are likely pathogenic in these hearts (and not secondary to cardiac dysfunction). This methodology led us to identify 501 coding and 208 noncoding as direct LMNA-regulated genes since their expression was completely rescued upon LMNA expression in the *Lmna*$^{-/-}$ mice. This study also identified 1862 coding and 607 lncRNA genes as partially rescued and dependent on LMNA for their expression and regulation.

Our study identified key upstream regulators of dysregulated transcripts namely KDM5A, TP53, and rapamycin-insensitive companion of mTOR, which were activated, and RB1, PITX2, and melanocyte-inducing transcription factor, which were suppressed. Of these, activation of the KDM5 family of proteins in the heart in laminopathies is a novel finding and was verified at the protein level. The induction of KDM5A expression was associated with suppression of its downstream targets, which included genes involved in mitochondrial biogenesis and function. These studies are also consistent with our previous data showing reduced mitochondrial electron transport complex I gene expression and enzymatic activity in the *Lmna*$^{-/-}$ mouse hearts.[17] Recent studies have also shown induction of KDM5A in other forms of cardiomyopathies associated with suppression of mitochondrial activity and oxidative phosphorylation, thereby underscoring the role of KDM5 in cardiac energy homeostasis in the context of heart failure.[39]

Furthermore, our analysis identified several transcriptional regulators, including E2F, TP53, and forkhead box Os that were previously implicated in the laminopathies.[13,14,17,19] These altered regulators identified in the present study collectively regulate numerous biological processes relevant to laminopathies, including cell proliferation, cell death, inflammation, and metabolism, among others. These transcriptional factors were regulated by LMNA, as reexpression of LMNA in the *Lmna*$^{-/-}$ mice partially or reverted the regulators toward normal WT levels.

Gene expression analysis also showed that the cell death/apoptosis signature, which was induced upon LMNA loss, could not be rescued upon AAV9 treatment. These gene expression data were consistent with increased TUNEL positive cells in the *Lmna*$^{-/-}$ hearts that could not be rescued by AAV9 treatment. Expression of the differentially expressed lncRNA correlated with those of the coding RNAs. A subset of these lncRNAs correlated highly with the expression of mRNAs that are targeted by the upstream regulators such as TP53 and KDM5A. Additional studies would be required to delineate the role of TP53 and KDM5A in the regulation of lncRNAs and their biological functions in the heart and to substantiate their pathogenic roles in cardiac dysfunction associated with laminopathies.

The study has several limitations. Notable among them is that RNA sequencing was performed on whole heart RNA rather than in isolated cardiac myocyte RNA. Therefore, the observed transcriptomic changes in the *Lmna*$^{-/-}$ mouse hearts originated from multiple cell types in the heart that are deficient in the LMNA protein. However, the rescue experiments with the recombinant AAV9 viruses results in re-expression of the LMNA protein mainly in cardiac myocytes and to a lesser extent, if at all, in other cell types. Whole heart RNA sequencing was adopted, as opposed to cardiac myocyte RNA sequencing, to determine global changes in the transcript levels, comprised of changes in the transduced cardiac myocytes and those in nonmyocyte cells, the latter encompassing the paracrine effects originating from transduced cardiac myocytes. The approach is not expected to rescue differentially expressed genes originating from nontransduced cardiac cells which likely are non-cardiac myocyte cells in the heart. This limitation might in part explain the incomplete phenotypic rescue in the *Lmna*$^{-/-}$ mice. Consistent with this notion, cardiac fibrosis in the *Lmna*$^{-/-}$ mice was not affected upon AAV9 gene transfer, reflective of the ineffective transduction of cardiac fibroblasts with the AAV9 viruses. Similarly, apoptosis, as assessed by the TUNEL assay, was not rescued, likely indicative of cell death occurring in non-myocyte LMNA-deficient cells in the heart. Partial rescue of cardiac function despite the lack of an effect on apoptosis, points to a direct role of the LMNA in cardiac myocyte contractile function. While we surmise that apoptosis involved non-myocyte cells, accurate identification of the cell type undergoing apoptosis remains unknown. Therefore, contributions of various cell types to the pathogenesis of cardiac phenotype in LMNA-deficiency could not be accurately ascertained in the present study, but it is reasonable to conclude that cardiac myocytes are the major contributors to cardiac dysfunction and impaired survival in the LMNA-deficient mice. Finally, the AAV9 virus is known to be highly cardiotrophic especially at the dose used in the present study. Nevertheless, other cell types such as skeletal muscles might be transduced as well and contribute to phenotypic rescue.

RNA sequencing data showed a preponderance of partially rescued genes upon AAV9-Lmna^{WT} treatment. This was also associated with variability in the gene expression as observed in the RNA sequencing and subsequent quantitative polymerase chain reaction experiments. Several factors may account for these observations, among them is that even though AAV9 has a well-established tropism toward cardiac myocytes, the transduction efficiency was incomplete and to some extent heterogeneous among myocytes and in myocardial regions. Consequently, transduction with the recombinant AAV9 viruses leads to variable expression of the transgene among hearts and animals, and maybe one reason for the partial rescue of the phenotype. Furthermore, since LMNA regulates gene expression through multiple mechanisms the threshold of LMNA expression required to achieve complete reversal might be variable, dependent on a gene by gene basis, and may account for the partial rescue in gene expression pattern and ensuing phenotypes. In this study the numbers of the animals in the experimental group were not sufficiently large to conclusively determine the correlation between the expression level of the transgene and the partially rescued phenotypes such as survival or cardiac function.

The mechanism, by which LMNA influences gene expression, including expression of lncRNAs, is not fully understood and seemingly involves multiple mechanisms. Our study identifies KDM5A and KDM5B, and TP53 as the potential regulators. Future studies would be required to delineate the mechanism(s) responsible for the upregulation of KDM5A and KDM5B in the heart in DCM and determine their pathogenic roles in DCM associated with laminopathies. Nevertheless, transcriptomic restoration was sufficient to improve survival and cardiac function and to some extent reduce cell death. Collectively, the approach enabled the identification of the dysregulated transcriptome and the upstream regulators that are regulated by LMNA in the heart, independent of cardiac dysfunction in the *Lmna*$^{-/-}$ mice.

Taken together, our data point to the role of LMNA in regulating expression of coding and non-coding RNAs in the heart and identify activation of KDM5A and KDM5B, TP53, and rapamycin-insensitive companion of mTOR and suppression of RB1, PITX2 and melanocyte-inducing transcription factor in the LMNA deficient hearts. These findings could serve as a platform for gaining mechanistic insights into the pathogenesis of the cardiac phenotypes in laminopathies, including cardiomyopathy, cardiac arrhythmias, and cardiac conduction defects.

ARTICLE INFORMATION

Received December 18, 2019; accepted June 19, 2020.

Affiliations

From the Center for Cardiovascular Genetics, Institute of Molecular Medicine, University of Texas Health Sciences Center at Houston, TX (J.C.P., G.A., R.L., S.N.C., T.G., A.J.M., P.G.), Center for Cardiovascular Research, St Louis, MO (S.J.M.); Cardiovascular Institute, Icahn School of Medicine at Mount Sinai, New York, NY (K.C., J.M.R., T.W.); MD Anderson Cancer Center, Houston, TX (S.K.S.); and Baylor College of Medicine, Houston, TX (M.J.R., C.C.).

Sources of Funding

This work was supported in part by grants from NIH (NIA, R21 AG060413-01, NHLBI, R01 HL088498 and 1R01HL132401), Leducq Foundation (14 CVD 03), The Welch Foundation, The Ewing Halsell Foundation, and George and Mary Josephine Hamman Foundation.

Disclosures

None.

Supplementary Materials

Data S1
Tables S1-S8
Figures S1–S5
Reference 40

REFERENCES

1. Capell BC, Collins FS. Human laminopathies: nuclei gone genetically awry. *Nat Rev Genet*. 2006;7:940–952.
2. Fatkin D, MacRae C, Sasaki T, Wolff MR, Porcu M, Frenneaux M, Atherton J, Vidaillet HJ Jr, Spudich S, De Girolami U, et al. Missense mutations in the rod domain of the lamin A/C gene as causes of dilated cardiomyopathy and conduction-system disease. *N Engl J Med*. 1999;341:1715–1724.
3. Schreiber KH, Kennedy BK. When lamins go bad: nuclear structure and disease. *Cell*. 2013;152:1365–1375.
4. Worman HJ, Bonne G. "Laminopathies": a wide spectrum of human diseases. *Exp Cell Res*. 2007;313:2121–2133.
5. Quarta G, Syrris P, Ashworth M, Jenkins S, Zuborne Alapi K, Morgan J, Muir A, Pantazis A, McKenna WJ, Elliott PM. Mutations in the lamin A/C gene mimic arrhythmogenic right ventricular cardiomyopathy. *Eur Heart J*. 2012;33:1128–1136.
6. Taylor MR, Fain PR, Sinagra G, Robinson ML, Robertson AD, Carniel E, Di Lenarda A, Bohlmeyer TJ, Ferguson DA, Brodsky GL, et al. Natural history of dilated cardiomyopathy due to lamin A/C gene mutations. *J Am Coll Cardiol*. 2003;41:771–780.
7. Anselme F, Moubarak G, Savoure A, Godin B, Borz B, Drouin-Garraud V, Gay A. Implantable cardioverter-defibrillators in lamin A/C mutation carriers with cardiac conduction disorders. *Heart Rhythm*. 2013;10:1492–1498.
8. van Berlo JH, Duboc D, Pinto YM. Often seen but rarely recognised: cardiac complications of lamin A/C mutations. *Eur Heart J*. 2004;25:812–814.
9. Guelen L, Pagie L, Brasset E, Meuleman W, Faza MB, Talhout W, Eussen BH, de Klein A, Wessels L, de Laat W, et al. Domain organization of human chromosomes revealed by mapping of nuclear lamina interactions. *Nature*. 2008;453:948–951.
10. Kind J, Pagie L, Ortabozkoyun H, Boyle S, de Vries SS, Janssen H, Amendola M, Nolen LD, Bickmore WA, van Steensel B. Single-cell dynamics of genome-nuclear lamina interactions. *Cell*. 2013;153:178–192.
11. Perovanovic J, Dell'Orso S, Gnochi VF, Jaiswal JK, Sartorelli V, Vigouroux C, Mamchaoui K, Mouly V, Bonne G, Hoffman EP. Laminopathies disrupt epigenomic developmental programs and cell fate. *Sci Transl Med*. 2016;8:335ra358.
12. van Steensel B, Belmont AS. Lamina-associated domains: links with chromosome architecture, heterochromatin, and gene repression. *Cell*. 2017;169:780–791.
13. Cheedipudi SM, Matkovich SJ, Coarfa C, Hu X, Robertson MJ, Sweet M, Taylor M, Mestroni L, Cleveland J, Willerson JT, et al. Genomic reorganization of lamin-associated domains in cardiac myocytes is associated with differential gene expression and DNA methylation in human dilated cardiomyopathy. *Circ Res*. 2019;124:1198–1213.
14. Brayson D, Shanahan CM. Current insights into lmna cardiomyopathies: Existing models and missing lincs. *Nucleus*. 2017;8:17–33.
15. Lund EG, Duband-Goulet I, Oldenburg A, Buendia B, Collas P. Distinct features of lamin A-interacting chromatin domains mapped by ChIP-sequencing from sonicated or micrococcal nuclease-digested chromatin. *Nucleus*. 2015;6:30–39.
16. Paulsen J, Sekelja M, Oldenburg AR, Barateau A, Briand N, Delbarre E, Shah A, Sorensen AL, Vigouroux C, Buendia B, et al. Chrom3D: three-dimensional genome modeling from Hi-C and nuclear lamin-genome contacts. *Genome Biol*. 2017;18:21.
17. Auguste G, Gurha P, Lombardi R, Coarfa C, Willerson JT, Marian AJ. Suppression of activated FOXO transcription factors in the heart prolongs survival in a mouse model of laminopathies. *Circ Res*. 2018;122:678–692.
18. Worman HJ. Nuclear lamins and laminopathies. *J Pathol*. 2012;226:316–325.
19. Chen SN, Lombardi R, Karmouch J, Tsai JY, Czernuszewicz G, Taylor MRG, Mestroni L, Coarfa C, Gurha P, Marian AJ. DNA damage response/TP53 pathway is activated and contributes to the pathogenesis of dilated cardiomyopathy associated with LMNA (lamin A/C) mutations. *Circ Res*. 2019;124:856–873.
20. Nikolova V, Leimena C, McMahon AC, Tan JC, Chandar S, Jogia D, Kesteven SH, Michalicek J, Otway R, Verheyen F, et al. Defects in nuclear structure and function promote dilated cardiomyopathy in lamin A/C-deficient mice. *J Clin Invest*. 2004;113:357–369.
21. Nikolova-Krstevski V, Leimena C, Xiao XH, Kesteven S, Tan JC, Yeo LS, Yu ZY, Zhang Q, Carlton A, Head S, et al. Nesprin-1 and actin contribute to nuclear and cytoskeletal defects in lamin A/C-deficient cardiomyopathy. *J Mol Cell Cardiol*. 2011;50:479–486.
22. Sullivan T, Escalante-Alcalde D, Bhatt H, Anver M, Bhat N, Nagashima K, Stewart CL, Burke B. Loss of a-type lamin expression compromises nuclear envelope integrity leading to muscular dystrophy. *J Cell Biol*. 1999;147:913–920.
23. Cheedipudi SM, Hu J, Fan S, Yuan P, Karmouch J, Czernuszewicz G, Robertson MJ, Coarfa C, Hong K, Yao Y, et al. Exercise restores dysregulated gene expression in a mouse model of arrhythmogenic cardiomyopathy. *Cardiovasc Res*. 2020;116:1199–1213.
24. Devereux RB, Alonso DR, Lutas EM, Gottlieb GJ, Campo E, Sachs I, Reichek N. Echocardiographic assessment of left ventricular hypertrophy: comparison to necropsy findings. *Am J Cardiol*. 1986;57:450–458.
25. Gurha P, Chen X, Lombardi R, Willerson JT, Marian AJ. Knockdown of plakophilin 2 downregulates miR-184 through CpG hypermethylation and suppression of the E2F1 pathway and leads to enhanced adipogenesis in vitro. *Circ Res*. 2016;119:731–750.
26. Trapnell C, Pachter L, Salzberg SL. TopHat: discovering splice junctions with RNA-Seq. *Bioinformatics*. 2009;25:1105–1111.
27. Anders S, Pyl PT, Huber W. HTSeq—a Python framework to work with high-throughput sequencing data. *Bioinformatics*. 2015;31:166–169.
28. Law CW, Alhamdoosh M, Su S, Smyth GK, Ritchie ME. RNA-seq analysis is easy as 1-2-3 with limma, Glimma and edgeR. *F1000Res*. 2016;5:1408.
29. Liberzon A, Subramanian A, Pinchback R, Thorvaldsdottir H, Tamayo P, Mesirov JP. Molecular signatures database (MSigDB) 3.0. *Bioinformatics*. 2011;27:1739–1740.
30. Subramanian A, Tamayo P, Mootha VK, Mukherjee S, Ebert BL, Gillette MA, Paulovich A, Pomeroy SL, Golub TR, Lander ES, et al. Gene set enrichment analysis: a knowledge-based approach for

interpreting genome-wide expression profiles. *Proc Natl Acad Sci USA*. 2005;102:15545–15550.
31. Bergmann O, Zdunek S, Alkass K, Druid H, Bernard S, Frisen J. Identification of cardiomyocyte nuclei and assessment of ploidy for the analysis of cell turnover. *Exp Cell Res*. 2011;317:188–194.
32. Gilsbach R, Preissl S, Gruning BA, Schnick T, Burger L, Benes V, Wurch A, Bonisch U, Gunther S, Backofen R, et al. Dynamic DNA methylation orchestrates cardiomyocyte development, maturation and disease. *Nat Commun*. 2014;5:5288.
33. Preissl S, Schwaderer M, Raulf A, Hesse M, Gruning BA, Kobele C, Backofen R, Fleischmann BK, Hein L, Gilsbach R. Deciphering the epigenetic code of cardiac myocyte transcription. *Circ Res*. 2015;117:413–423.
34. Ishikawa K, Tilemann L, Fish K, Hajjar RJ. Gene delivery methods in cardiac gene therapy. *J Gene Med*. 2011;13:566–572.
35. Prasad KM, Xu Y, Yang Z, Acton ST, French BA. Robust cardiomyocyte-specific gene expression following systemic injection of AAV: in vivo gene delivery follows a Poisson distribution. *Gene Ther*. 2011;18:43–52.
36. Pacak CA, Mah CS, Thattaliyath BD, Conlon TJ, Lewis MA, Cloutier DE, Zolotukhin I, Tarantal AF, Byrne BJ. Recombinant adeno-associated virus serotype 9 leads to preferential cardiac transduction in vivo. *Circ Res*. 2006;99:e3–e9.
37. de Leeuw R, Gruenbaum Y, Medalia O. Nuclear lamins: thin filaments with major functions. *Trends Cell Biol*. 2018;28:34–45.
38. Jacob KN, Garg A. Laminopathies: multisystem dystrophy syndromes. *Mol Genet Metab*. 2006;87:289–302.
39. Chen L, Yang F, Chen X, Rao M, Zhang NN, Chen K, Deng H, Song JP, Hu SS. Comprehensive myocardial proteogenomics profiling reveals C/EBPalpha as the key factor in the lipid storage of ARVC. *J Proteome Res*. 2017;16:2863–2876.
40. Kohlbrenner E, Henckaerts E, Rapti K, Gordon RE, Linden RM, Hajjar RJ, Weber T. Quantification of AAV particle titers by infrared fluorescence scanning of coomassie-stained sodium dodecyl sulfate-polyacrylamide gels. *Hum Gene Ther Methods*. 2012;23:198–203.

SUPPLEMENTAL MATERIAL

Data S1.

SUPPLEMENTAL METHODS

Recombinant constructs:

We utilized a Flag-tagged *Lmna* construct to detect and establish the efficiency of transduction, devoid of potential confounding effects of any residual endogenous LMNA protein. The non-tagged *Lmna* construct was subsequently used for gene expression and phenotypic studies in the pTRU11 vectors (Figure S1). Sanger sequencing confirmed proper insertion and sequence integrity of the clones. To create a plasmid that allows the production of AAV with a genome without an expression cassette, the CAG promoter was eliminated from pTREK3 (a kind gift of Dr. Michael Linden) by digesting pTREK3 with EcoRI followed by vector re-ligation yielding the plasmid pTR-GNPR. The pTR-GNPR plasmid was then digested with Sbf*I* and Kpn*I* and a Sbf*I*/Kpn*I* fragment from pCherry-Luciferase was inserted yielding pTR-No-Cassette. pTR-NoCassette can be used to create recombinant AAVs with an approximately 4.2 kb long vector genome without an expression cassette.

All ITR containing plasmids were maintained in SURE2 cells (Agilent; Santa Clara, CA) and were grown at 30 °C in LB broth with 100ug/ml ampicillin. pDG9 was maintained in DH5α (Thermo Fisher Scientific; Waltham, MA) cells and grown at 37 °C in LB broth with 100ug/ml ampicillin. Plasmid DNA for transfections was prepared using a Zymo pure maxi prep kit (Zymo Research; Irvine, CA) according to the manufacturer's instructions. AAV9 encoding LMNA was prepared as described with minor modifications [40]. In lieu of the polyethyleneimine (PEI) solution, the transfection was performed using PEI-Max 160 kD (Polysciences; Warrington, PA). The PEI-MAX solution was prepared by adding 100 mg PEI-MAX to PBS (without calcium and magnesium) while mixing with a magnetic stirrer. The pH was adjusted to pH 4.5 by the dropwise addition of 12N HCl. After stirring overnight, the solution was filtered (0.22 µm) and aliquots stored at -80 °C. Transfection of HEK293T cells was performed as described [40] in, except that, 250 µl of the PEI-Max solution was used instead of 700 µl of the PEI solution. The virus was purified and dialyzed against lactated Ringer's solution. Vector

genome titers (and genome integrity) were determined by alkaline gel electrophoresis and confirmed by qPCR using an ABI 7500 Real-Time PCR system (Thermo Fisher Scientific; Waltham, MA) and the iTaq Universal SYBR green supermix (Bio-Rad; Hercules, CA). As a qPCR standard, we used an internal reference standard virus that was calibrated against the AAV2 reference standard from ATCC (Manassas, VA)[40].

Table S1.

A. Oligonucleotide primers used for genotyping

Transgene	Sequence
Lmna	Forward: CAAGTCCCCATCACTTGGTT Forward: GCCAGAGGCCACTTGTGTAG Reverse: CTGTGACACTGGAGGCAGAA

B. Oligonucleotide primers used in qPCR reactions

Name	Sequence
Gapdh	Forward: TGGCAAAGTGGAGATTGTTGC Reverse: AAGATGGTGATGGGCTTCCCG
Lmna	Forward: TCCCACCGAAGTTCACCCTA Reverse: TGGAGTTGATGAGAGCGGTG
Mrpl55	Forward: AGTAAAGTTCTGCACGGCG Reverse: TCACACCACAATGCCTCAG
Rpl3l	Forward: GTGATCACTCTGAGAAAGTC Reverse: CTTACATGTTTCCCAAGGTC
Mrpl12	Forward: GGCATCAACCTCGTCCAG Reverse: CCTCATAACCATGCCTCACTC
Sdhb	Forward: ACCCCTTCTCTGTCTACCG Reverse: AATGCTCGCTTCTCCTTGTAG
Dlst	Forward: TGATAACAGTCCAAACCCCAG Reverse: ACGGAACCTGCACAGAAG
Opa1	Forward: GTGTGCTGGAAATGATTGCTC Reverse: TGGTGAGATCAAATTCCCGAG
Uqcrfs1	Forward: TTCTGGATGTGAAGCGACC Reverse: GATAGTCAGAGAAGTCGGGC
Cdkn1a	Forward: CTGACAGATTTCTATCACTCC Reverse: TTAAGACACACAGAGTGAGG
Hmox1	Forward: CATGAAGAACTTTCAGAAGGG Reverse: TAGATATGGTACAAGGAAGCC
Hspb1	Forward: CTTCACCCGGAAATACAC Reverse: CGAAAGTAACCGGAATGG
Gpx3	Forward: ACAAGAGAAGTCTAAGACAGAC Reverse: TGTAGTGCATTCAGTTCAAG
Clu	Forward: CTTAAGAGAAGGTGAAGATGAC Reverse: CAGGATTGTTGGTTGAACAG
Fas	Forward: TGAATGCCTCAAATCTTAGC Reverse: TTTTAGCTTCCTGGATTGTC
Ctgf	Forward: GAGGAAAACATTAAGAAGGGC Reverse: AGAAAGCTCAAACTTGACAG

Table S2. Antibodies used for Immunoblot (IB) and Immunofluorescence (IF) studies.

Antibodies	Concentration	Supplier	Catalog number
Lamin A	1:1,000 (IF)	Millipore	MAB3540
PCM-1	1:1,000 (IF)	Sigma	HPA023370
FLAG	1:1,000 (IF)	Sigma	F3165
GAPDH	1:1,000 (IB)	Abcam	ab8245
Lamin A	1:1,000 (IB)	Abcam	ab26300
Lamin A/C	1:250 (IB)	Santa cruz	sc-376248
KDM5A	1:1,000 (IB)	Abcam	ab70892
KDM5B	1:1,000 (IB)	Novus	NB100-97821
EMERIN	1:1,000 (IB)	Santa Cruz	sc-25284
Anti-mouse IgG HRP linked antibody	1:5,000 (IB)	Cell Signaling Technology	# 7076
Anti-rabbit IgG HRP linked antibody	1:2,000 (IB)	Cell Signaling Technology	# 7074
Donkey anti-Mouse IgG, Alexa Fluor 488	1:1,000 (IF)	Invitrogen	A21202
Donkey anti-Rabbit IgG, Alexa Fluor 594	1:1,000 (IF)	Invitrogen	A21207

Table S3. Echocardiographic findings in WT, *Lmna*$^{-/-}$, *Lmna*$^{-/-}$:AAV9-vector and *Lmna*$^{-/-}$:AAV9-*Lmna*^{WT} at 2 weeks of age.

	WT	*Lmna*$^{-/-}$	*Lmna*$^{-/-}$-AAV9-*vector*	*Lmna*$^{-/-}$-AAV9-*Lmna*^{WT}	*p*
N	17	14	12	6	N/A
M/F	10/7	9/5	5/7	4/2	0.640$^{\chi}$
Age (days)	13.4±1.2	13.7±1.2	14.5±0.9	14.0±0.0	0.160
Body weight (g)	7.5±1.9	5.9±1.3	6.0±1.8	7.0±1.9	0.049
HR (bpm)	511±67	512±75	533±76	542±57	0.430
IVST(mm)	0.56±0.07	0.53±0.08	0.51±0.07	0.50±0.06	0.150
PWT (mm)	0.57±0.08	0.52±0.07	0.52±0.05	0.51±0.08	0.100
LVEDD (mm)	2.53±0.30	2.30±0.28	2.28±0.34	2.28±0.24	0.100
LVEDDi (mm/g)	0.35±0.07	0.40±0.06	0.40±0.08	0.34±0.08	0.140
LVESD (mm)	1.23±0.22	1.14±0.22	1.10±0.17	1.08±0.22	**0.280**
LVESDi (mm/g)	0.17±0.04	0.20±0.04	0.19±0.04	0.16±0.06	0.200
FS (%)	51.6±4.0	50.6±5.0	51.3±4.0	52.9±5.1	0.790
LVM (mg)	34±10	26±9	25±8	24±7	**0.030**
LVMi (mg/g)	4.6±1.3	4.5±1.3	4.2±0.6	3.70±1.5	**0.310**

χ Chi^2 test.

One-way ANOVA, with Tukey's pairwise comparison and Kruskal-Wallis (p-value marked in bold), with Dunn's correction, were used.

HR, heart rate; bpm, beats per minutes; IVST, interventricular septal thickness; PWT, posterior wall thickness; LVEDD, left ventricular end diastolic diameter; LVEDDi, LVEDD divided by the body weight; LVESD, left ventricular end systolic diameter; LVESDi , LVESD divided for the body weight; FS, fractional shortening; LVM, left ventricular mass; LVMi, LVM divided by the body weight.

Table S4. GSEA of rescued genes showing the status of hallmark signature in the indicated group. The significant gene sets are shown in bold.

	Lmna$^{-/-}$ vs WT		AAV9:*Lmna*$^{-/-}$ vs *Lmna*$^{-/-}$	
NAME	**NES**	**q**	**NES**	**q**
HALLMARK_TNFA_SIGNALING_VIA_NFKB	**3.4**	**<0.0001**	**-1.9**	**0.016**
HALLMARK_EPITHELIAL_MESENCHYMAL_TRANSITION	**2.9**	**<0.0001**	**-1.9**	**0.019**
HALLMARK_P53_PATHWAY	**2.3**	**0.005**	-1.3	0.128
HALLMARK_HYPOXIA	**2.2**	**0.004**	-13	0.244
HALLMARK_APOPTOSIS	**2.0**	**0.013**	-0.8	0.874
HALLMARK_INFLAMMATORY_RESPONSE	**1.9**	**0.025**	-1.3	0.250
HALLMARK_ANDROGEN_RESPONSE	**1.8**	**0.029**	-1.2	0.266
HALLMARK_APICAL_JUNCTION	1.6	0.073	**-1.9**	**0.026**
HALLMARK_ESTROGEN_RESPONSE_LATE	1.6	0.071	-0.8	0.834
HALLMARK_IL2_STAT5_SIGNALING	1.6	0.076	-1.5	0.142
HALLMARK_ESTROGEN_RESPONSE_EARLY	1.4	0.124	-0.9	0.778
HALLMARK_UV_RESPONSE_DN	1.3	0.240	-1.6	0.079
HALLMARK_MYOGENESIS	1.2	0.255	-1.0	0.534
HALLMARK_INTERFERON_GAMMA_RESPONSE	1.1	0.433	NC	NC
HALLMARK_UV_RESPONSE_UP	1.0	0.532	-1.0	0.582
HALLMARK_KRAS_SIGNALING_UP	1.0	0.526	NC	NC
HALLMARK_GLYCOLYSIS	0.9	0.532	NC	NC

	Lmna$^{-/-}$ vs WT		AAV9:*Lmna*$^{-/-}$ vs *Lmna*$^{-/-}$	
NAME	**NES**	**q**	**NES**	**q**
HALLMARK_OXIDATIVE_PHOSPHORYLATION	**-2.9**	**<0.0001**	**2.5**	**<0.0001**
HALLMARK_E2F_TARGETS	**-2.2**	**0.003**	**2.4**	**<0.0001**
HALLMARK_G2M_CHECKPOINT	**-2.1**	**0.003**	**1.7**	**0.033**
HALLMARK_MITOTIC_SPINDLE	**-2.0**	**0.009**	1.0	0.509
HALLMARK_FATTY_ACID_METABOLISM	**-1.9**	**0.019**	**1.7**	**0.032**
HALLMARK_ALLOGRAFT_REJECTION	-1.6	0.114	1.6	0.062
HALLMARK_MYC_TARGETS_V1	-1.6	0.100	**1.8**	**0.026**
HALLMARK_PEROXISOME	-1.3	0.257	NC	NC
HALLMARK_XENOBIOTIC_METABOLISM	-1.2	0.367	0.8	0.707
HALLMARK_MTORC1_SIGNALING	-1.1	0.445	1.4	0.147
HALLMARK_SPERMATOGENESIS	-1.1	0.465	1.3	0.188
HALLMARK_ADIPOGENESIS	-1.0	0.497	1.5	0.074
HALLMARK_BILE_ACID_METABOLISM	-0.9	0.683	1.1	0.431
HALLMARK_HEME_METABOLISM	-0.8	0.720	1.1	0.416
HALLMARK_DNA_REPAIR	-0.8	0.705	1.6	0.057

Table S5. Ingenuity pathway analysis of genes that show complete rescue upon AAV9-*Lmna*^{WT} treatment of *Lmna*$^{-/-}$ mice.

Upstream Regulators	Z-scores	Overlap p-values
TP53	3.3	$1.7x10^{-6}$
KDM5A	3.3	$1.6x10^{-6}$
HTT	2.0	$1.9x10^{-6}$
RB1	-3.2	$6.0X10^{-5}$
PPARGC1A	-2.4	0.099
STAT1	-2.3	0.094
IRF3	-2.2	0.181
TAL1	-2.2	0.061
CEBPB	-2.1	0.133
TAF4	-2.0	0.061
MITF	-2.0	0.352
PITX2	-2.0	0.129

Only transcriptional regulators that show Z-Score greater than or equal to 2.0 and less than or equal to -2.0 are shown. Corresponding overlap p-values are also shown. Z-Scores and p-values were obtained from IPA software.

Table S6. Differentially regulated upstream regulators.

Upstream Regulator	*Lmna*$^{-/-}$ vs WT	AAV9:*Lmna*^{WT} vs *Lmna*$^{-/-}$	AAV9:*Lmna*^{WT} vs WT
RICTOR	5.8	-4.5	unchanged
MAP4K4	4.4	-1.5	unchanged
NR3C2	4.3	unchanged	2.0
TGFB1	3.8	unchanged	2.0
TRAP1	3.6	-1.9	unchanged
GPER1	3.6	unchanged	2.4
PDGF BB	3.5	2.6	3.3
AR	3.2	unchanged	unchanged
NR3C1	3.1	-0.5	1.8
NORAD	3.0	unchanged	1.0
Pkc(s)	2.8	-1.2	unchanged
PKM	2.8	unchanged	unchanged
FLCN	2.8	unchanged	unchanged
HRAS	2.6	unchanged	unchanged
Irgm1	2.5	-2.8	unchanged
SMTNL1	2.4	unchanged	unchanged
TCR	2.4	-0.2	unchanged
ALOX5	2.4	unchanged	unchanged
BMP10	2.4	unchanged	unchanged
BMP7	2.2	-1.6	unchanged
TAZ	2.2	-0.9	unchanged
CYP2J2	2.2	unchanged	unchanged
MGAT5	2.2	unchanged	unchanged
GDF2	2.2	unchanged	unchanged
GNAQ	2.2	unchanged	unchanged
Calcineurin protein(s)	2.2	unchanged	-0.2
HTR2B	2.2	unchanged	unchanged
FBXW7	2.1	unchanged	unchanged
ERK	2.1	unchanged	2.4
TNF	2.1	unchanged	unchanged
VGLL3	2.0	unchanged	unchanged
APOE	-2.1	unchanged	-2.0
SETD2	-2.1	unchanged	unchanged
EFNA5	-2.1	unchanged	unchanged
MAT1A	-2.2	unchanged	unchanged
PCGEM1	-2.2	0.15	unchanged
ASAH1	-2.2	unchanged	unchanged
PLA2R1	-2.4	2.6	unchanged
PTP4A3	-2.4	unchanged	unchanged
SNCA	-2.6	3.1	0.6
PTGER2	-2.6	unchanged	unchanged
Ifnar	-2.6	4.4	unchanged
EFNA1	-2.7	unchanged	unchanged
TIMP3	-2.7	unchanged	-1.0
MTOR	-2.8	unchanged	unchanged
LIN9	-2.8	unchanged	unchanged
PKD1	-3.0	unchanged	0.5
PTEN	-3.1	2.9	unchanged
RABL6	-3.2	unchanged	unchanged
EFNA2	-3.2	unchanged	unchanged
STK11	-3.2	3.0	unchanged
HBA1/HBA2	-4.0	unchanged	unchanged
Hbb-b1	-4.0	2.1	unchanged
INSR	-4.4	2.3	unchanged

Table S7. Echocardiographic findings in WT, *Lmna*$^{-/-}$ and *Lmna* $^{-/-}$:AAV9-*Lmna*^{WT} at 4 weeks of age.

	WT	*Lmna*$^{-/-}$	*Lmna*$^{-/-}$-AAV9-*vector*	*Lmna*$^{-/-}$-AAV9-*Lmna*^{WT}	*p*
N	23	19	9	15	N/A
M/F	11/12	12/7	6/3	8/7	0.690$^{\chi}$
Age (days)	28.1±1.9	28.2±1.5	28.1±0.2	28.2±0.4	0.960
Body weight (g)	14.0±3.4	7.5±1.7 *	7.9±0.8 †	9.7±3.2 ‡	<0.0001
HR (bpm)	518±84	512±63	520±59	497±63	0.820
IVST (mm)	0.60±0.06	0.51±0.08 *	0.51±0.06 †	0.63±0.11 § #	<0.0001
PWT (mm)	0.61±0.09	0.50±0.07 *	0.48±0.08 †	0.62±0.08 § #	**<0.0001**
LVEDD (mm)	3.25±0.29	2.70±0.42 *	2.77±0.22 †	2.67±0.39 ‡	**<0.0001**
LVEDDi mm/g)	0.24±0.05	0.37±0.07 *	0.35±0.03 †	0.29±0.05 §	**<0.0001**
LVESD (mm)	1.53±0.24	1.77±0.50	1.83±0.35	1.43±0.27 § #	**0.006**
LVESDi (mm/g)	0.12±0.03	0.24±0.04 *	0.23±0.03 †	0.16±0.04 ‡ § #	<0.0001
FS (%)	53.0±6.5	35.3±7.6 *	34.3±8.4 †	46.3±15.7 ‡§ #	<0.0001
LVM (mg)	55±11	33±14 *	32±5†	43±16	**<0.0001**
LVMi (mg/g)	4.1±0.8	4.3±0.9	4.0±0.6	4.4±0.5	0.550

χ Chi^2 test.

One-way ANOVA, with Tukeys pairwise comparison and Kruskal-Wallis (p-value marked in bold), with Dunn's correction, were used, with:

WT *vs Lmna*$^{-/-}$ * p <0.05

WT *vs Lmna*$^{-/-}$-AAV9-vector: † $p < 0.05$

WT *vs Lmna*$^{-/-}$-AAV9-*Lmna*^{WT} ‡ $p < 0.05$

Lmna$^{-/-}$ *vs Lmna*$^{-/-}$-AAV9-Lmna^{WT} § $p < 0.05$

Lmna$^{-/-}$-AAV9-vector *vs Lmna*$^{-/-}$-AAV9-Lmna^{WT} # $p < 0.05$

HR, heart rate; bpm, beats per minutes; IVST, interventricular septal thickness; PWT, posterior wall thickness; LVEDD, left ventricular end diastolic diameter; LVEDDi, LVEDD divided by the body weight; LVESD, left ventricular end systolic diameter; LVESDi , LVESD divided for the body weight; FS, fractional shortening; LVM, left ventricular mass; LVMi, LVM divided by the body weight.

Table S8. Echocardiographic findings in WT, *Lmna*$^{-/-}$ and *Lmna* $^{-/-}$: AAV9- *Lmna* ^{Flag} at 4 weeks of age.

	WT	***Lmna*** $^{-/-}$	***Lmna*** $^{-/-}$***:AAV9- Lmna Flag***	***p***
N	23	19	8	N/A
M/F	11/12	12/7	3/5	
Age (days)	28.1 ± 1.9	28.2 ± 1.5	27.0 ± 0.0	0.190
Body weight (g)	14.0 ± 3.5	7.5 ± 1.8 ****	7.4 ± 1.4 ‡‡‡‡	<0.0001
HR (bpm)	518 ± 86	512 ± 65	513 ± 75	0.964
IVST(mm)	0.60 ± 0.06	0.51 ± 0.08 ***	0.60 ± 0.08 §	0.0002
PWT (mm)	0.61 ± 0.10	0.50 ± 0.07 ***	0.53 ± 0.08	**0.0003**
LVEDD (mm)	3.25 ± 0.29	2.70 ± 0.43 ***	2.44 ± 0.34 ‡‡‡‡	**< 0.0001**
LVEDDi (mm/g)	0.24 ± 0.05	0.37 ± 0.07 ****	0.33 ± 0.04 ‡‡	**< 0.0001**
LVESD (mm)	1.53 ± 0.24	1.77 ± 0.51	1.32 ± 0.23 §§	**0.057**
LVESDi (mm/g)	0.12 ± 0.03	0.24 ± 0.04 ****	0.18 ± 0.03 ‡	**< 0.0001**
FS (%)	53.0 ± 6.6	35.3 ± 7.8 ****	45.9 ± 4.0 ‡ §§	< 0.0001
LVM (mg)	55 ± 12	33 ± 14 ****	31 ± 7 ‡‡‡	**< 0.0001**
LVMi (mg/g)	4.1 ± 0.9	4.3 ± 0.9	4.2 ± 0.7	0.679

One-way ANOVA, with Tukeys pairwise comparison and Kruskal-Wallis (p-value marked in bold), with Dunn's correction, were used, with:

WT *vs Lmna*$^{-/-}$ ***: p <0.001; ****: p < 0.0001

WT *vs Lmna*$^{-/-}$-AAV9- *Lmna*^{Flag} ‡: p < 0.05; ‡‡: p < 0.01; ‡‡‡: p < 0.001; ‡‡‡‡ : p < 0.0001

Lmna$^{-/-}$ *vs Lmna*$^{-/-}$-AAV9- *Lmna*^{Flag} §: p < 0.05; §§: p < 0.01

Abbreviations: HR, heart rate; bpm, beats per minutes; IVST, interventricular septal thickness; PWT, posterior wall thickness; LVEDD, left ventricular end diastolic diameter; LVEDDi, LVEDD divided by the body weight; LVESD, left ventricular end systolic diameter; LVESDi , LVESD divided for the body weight; FS, fractional shortening; LVM, left ventricular mass; LVMi, LVM divided by the body weight.

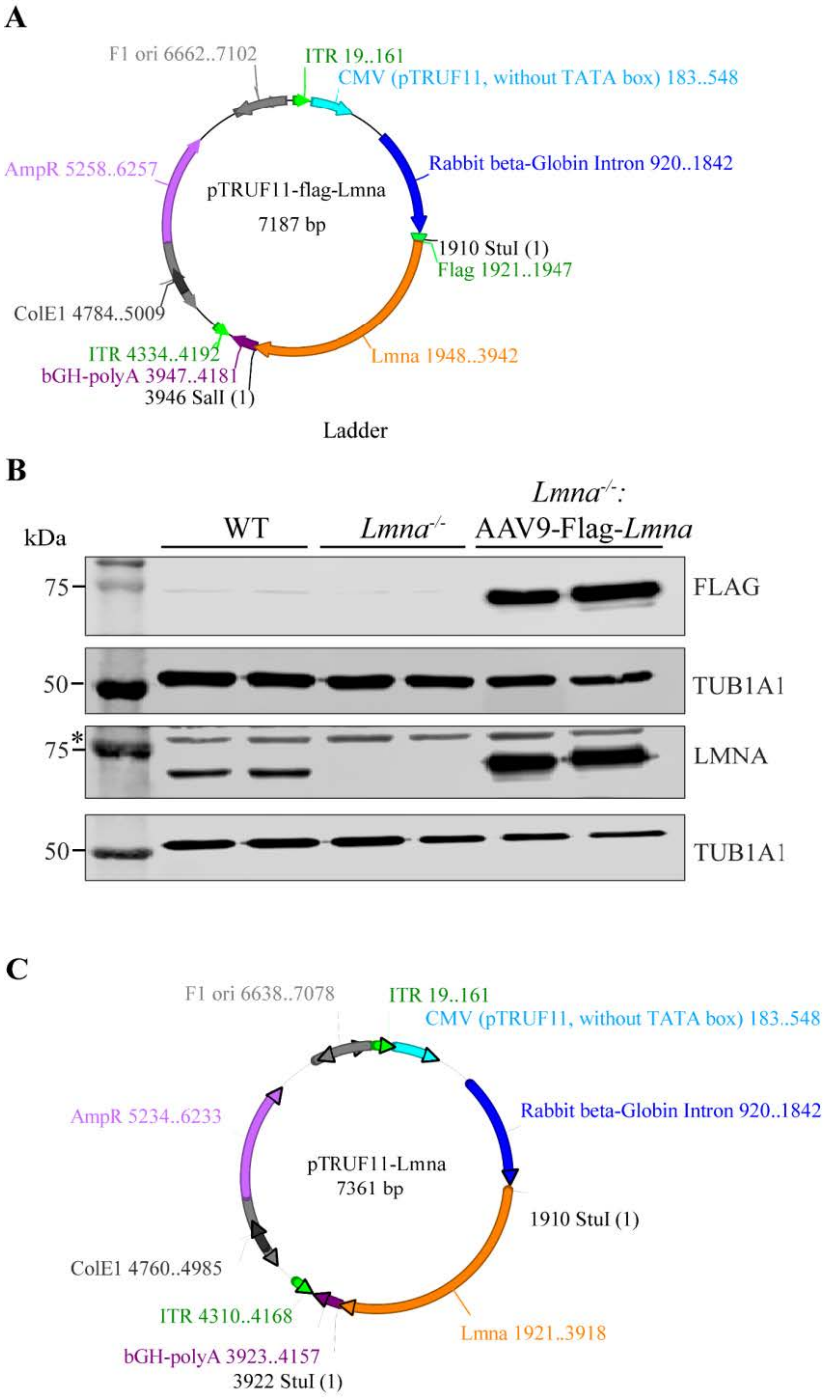

Figure S1:

A)Vector map for full-length wild-type and N-terminally Flag-tagged murine *Lmna* cDNAs cloned into a pTRUF11 plasmid downstream to a TATA-less CMV promoter and rabbit beta-globin intron at the StuI cloning site for AAV9 virus mediated expression in heart. **B)** AAV9-*Flag Lmna* was injected in neonatal *Lmna*$^{-/-}$ mice at P2,P4 and P6 and immuno blot anlaysis of whole heart samples from indicated genotype was perfomed to evaluate FLAG-LMNA expression in heart. Anti Lamin antibody recognize LMNA. * indicate non specific band (n=2) .**C)** Vector map for *Lmna* ^{WT} (without Flag tag) in pTRUF11 vector for subsequent AAV9 mediated expression in heart.

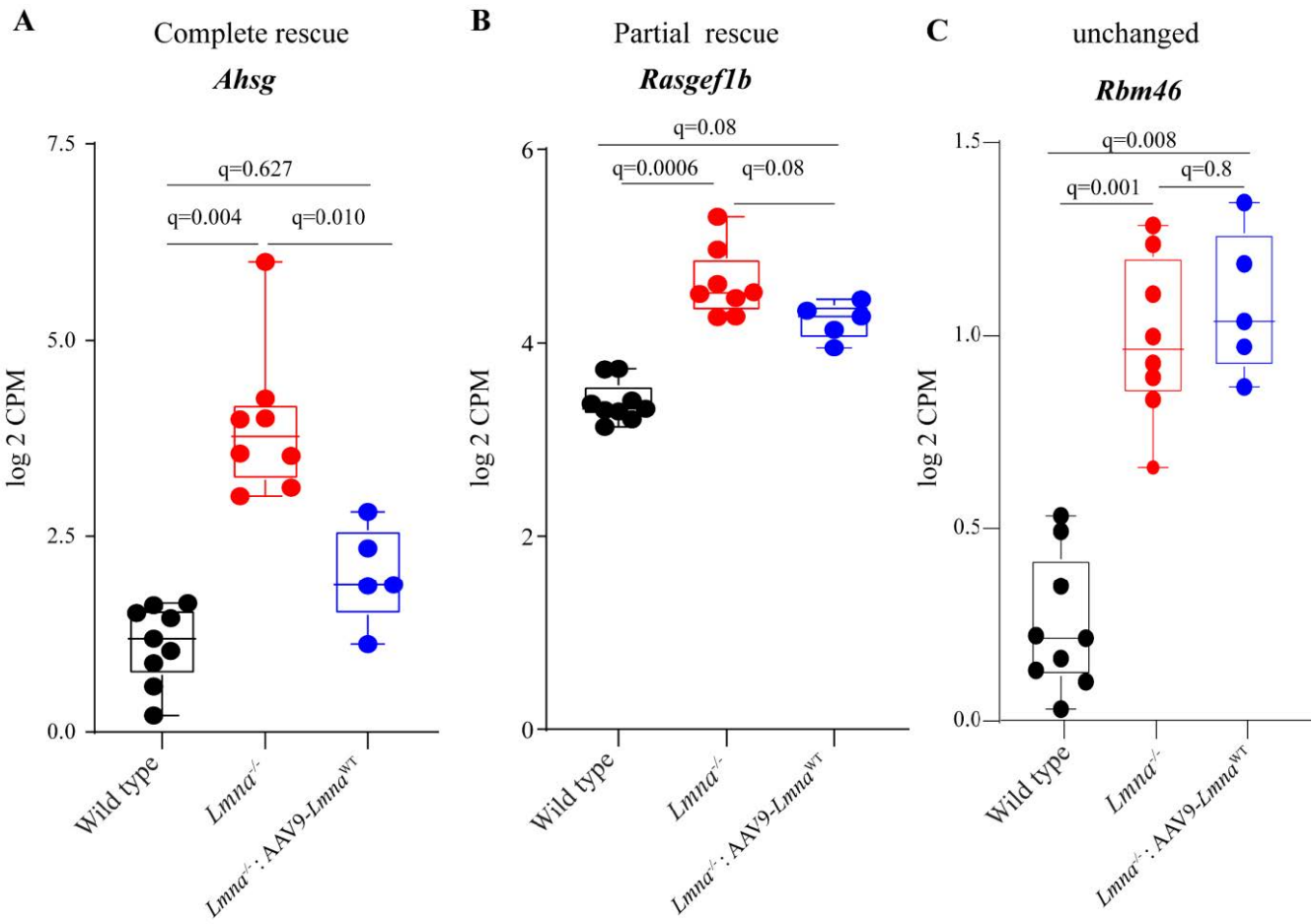

Figure S2: Graph showing log2CPM values obtained from RNA-seq data for WT, *Lmna*$^{-/-}$ and *Lmna*$^{-/-}$: AAV9-*Lmna*^{WT} mice .The status of differential expression between the indicated groups and panels are shown as an example for A) completely rescued B) partially rescued and C) unchanged gene. Adjusted p-values (i.e q) obtained from RNA-seq analysis are shown for each comparisions.

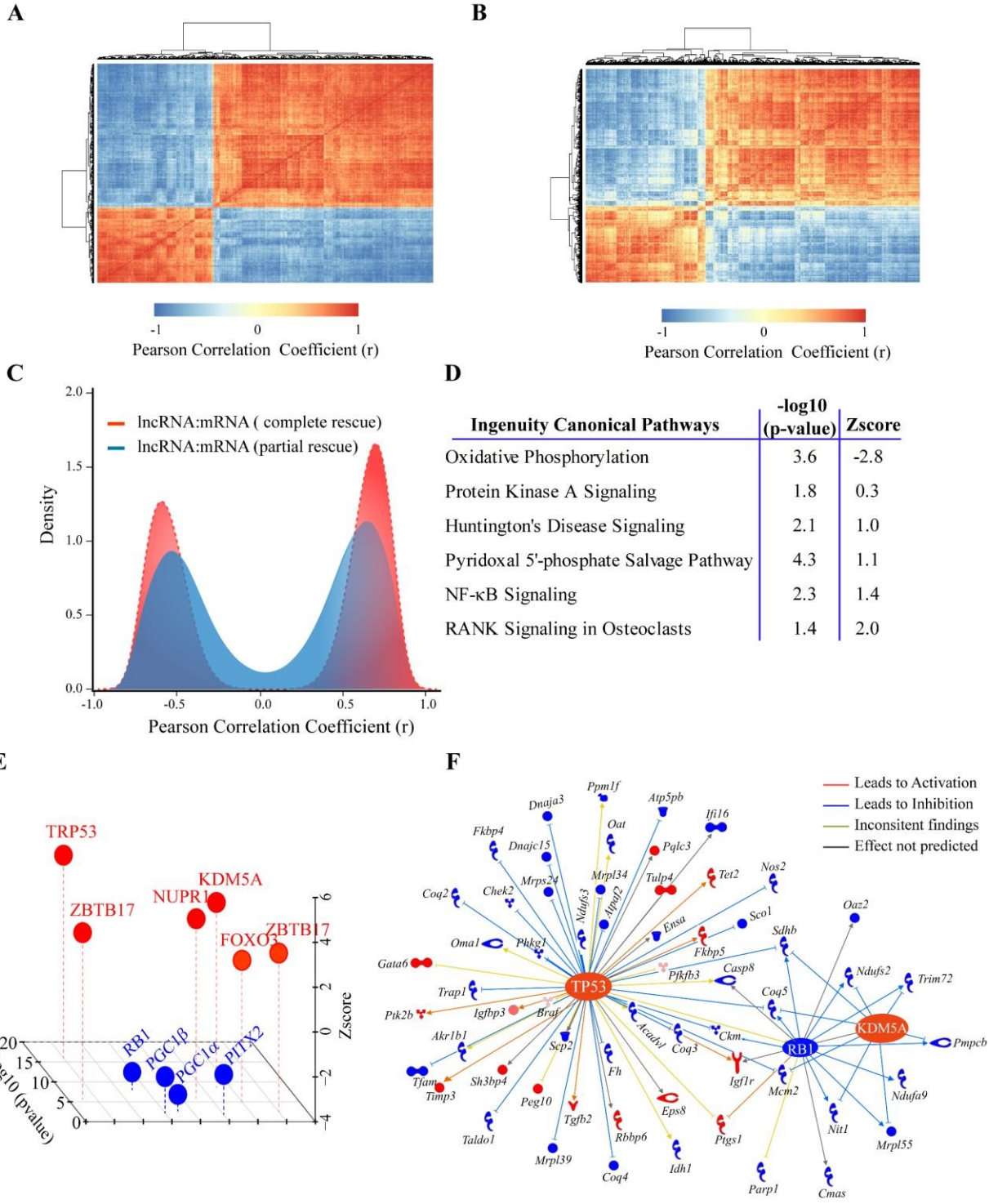

Ingenuity Canonical Pathways	-log10 (p-value)	Zscore
Oxidative Phosphorylation	3.6	-2.8
Protein Kinase A Signaling	1.8	0.3
Huntington's Disease Signaling	2.1	1.0
Pyridoxal 5'-phosphate Salvage Pathway	4.3	1.1
NF-κB Signaling	2.3	1.4
RANK Signaling in Osteoclasts	1.4	2.0

Figure S3: Correlation analysis of differentially expressed lncRNA and mRNAs in the *Lmna*$^{-/-}$ mice and upon *Lmna* ^{WT} re-expression: Heat map of correlation matrix between differentially expressed and completely rescued **(A)** and partially rescued **(B)** lncRNAs and mRNA. Correlation coefficient values for lncRNA:lncRNA, mRNA:mRNA and lncRNA:mRNA pair plotted as a heat map. **C)** Density plot for only lncRNA: mRNA pairs showing the distribution of correlation coefficient (r) for completely rescued and partially rescued lncRNA: mRNA pairs. **D-E)** IPA analysis for for caninical pathways (**D**) and Upstream regulators **(E)** for the most highly correlated complete and partially rescued mRNAs (r=0.9/-0.9). **F)** IPA interaction pathway map for upstream regulators identified in E showing the enrichment of mRNA targets and their coregulation. Only completely rescued genes are shown.

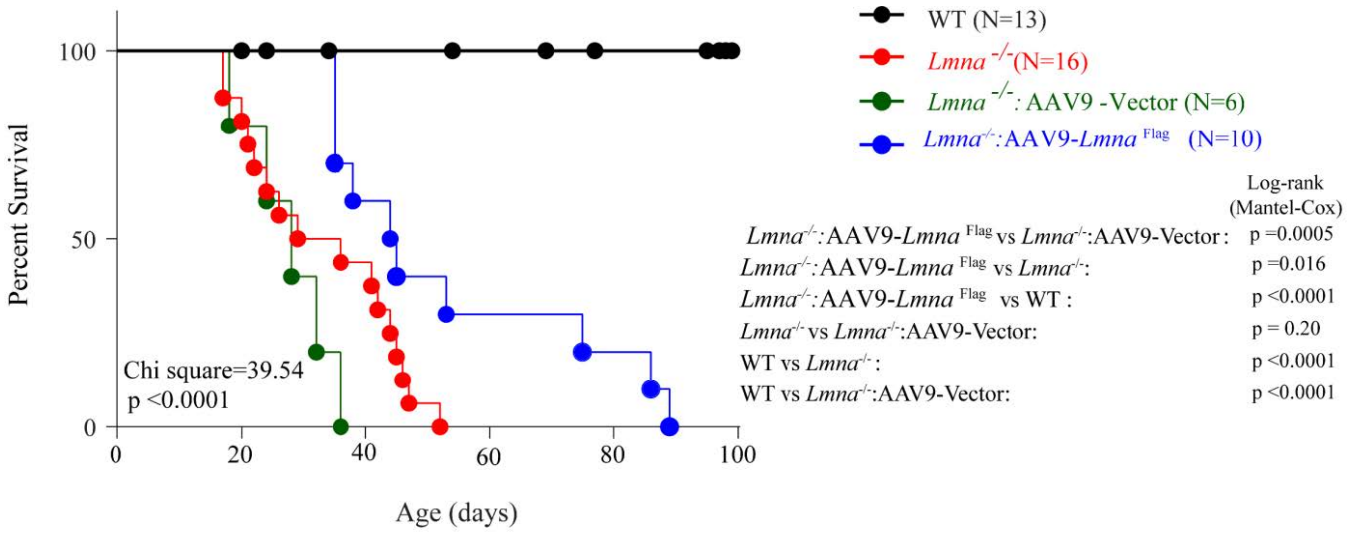

Figure S4: Kaplan-Meier survival plots for the mice in the indicated experimental group showing increase in survival of *Lmna*$^{-/-}$:AAV9-*Lmna*^{Flag} as compared to *Lmna*$^{-/-}$ or *Lmna:*AAV9-*Vector* group. Chi-square and p-value for the overall Kaplan Meier survival analysis are indicated in bold. Log-rank (Mantel-Cox) pairwise p-values for each subgroup analysis are shown.Kaplain meier survival plots and p-values were obtained from GraphPad prism software.

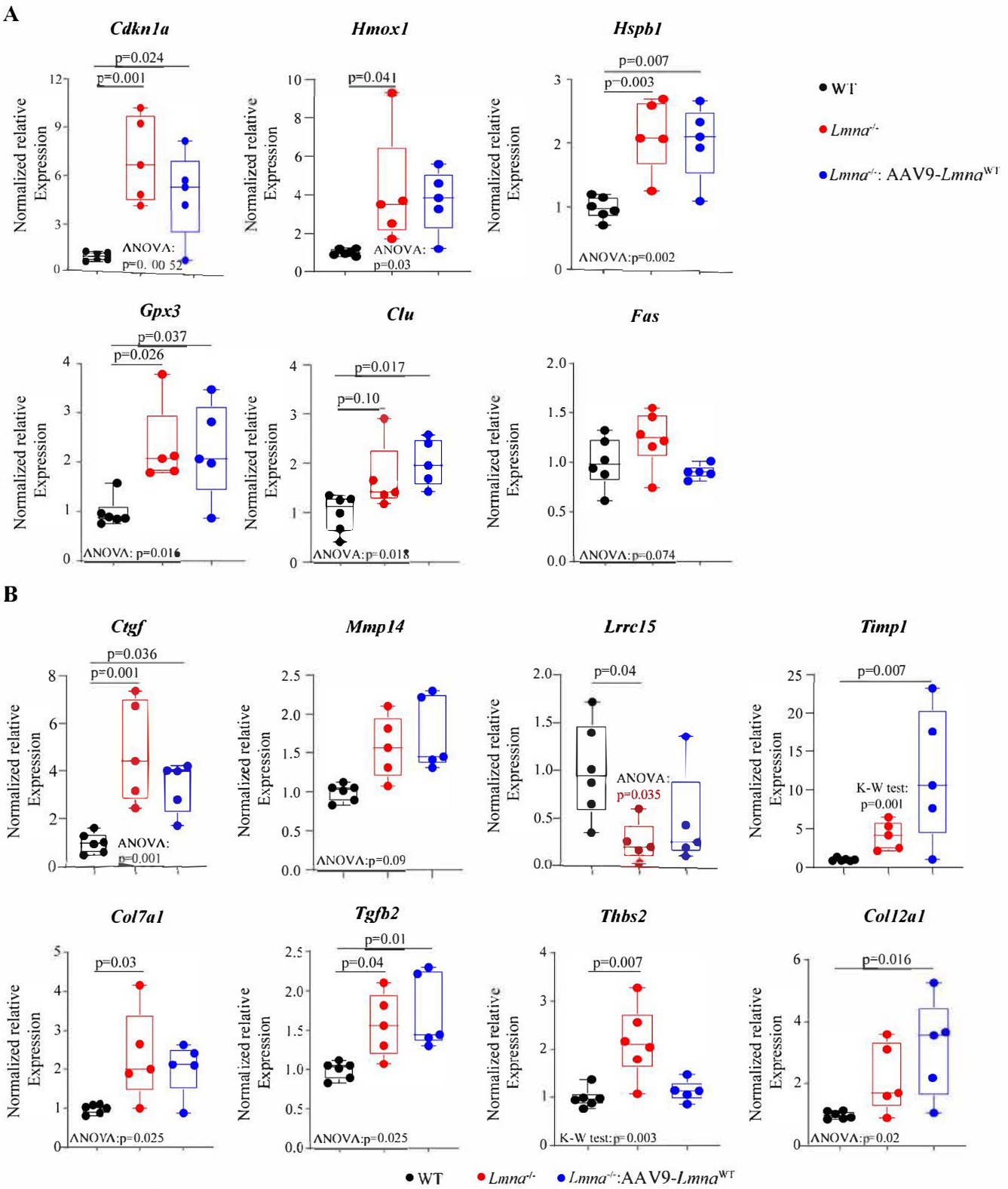

Figure S5: QPCR analysis of selected genes involved in cell death **(A)** and cardiac fibrosis **(B)** showing partial or no rescue upon AAV9-*Lmna*^{WT} treatment. For normally distributed dataset One-way ANOVA followed by Tukey's Posthoc test for multiple comparision was performed and Krushal-Wallis (K-W) test and Dunn's Posthoc test for multiple comparision was performed for once that deviated from normal distribution. Only p-values that were significant ($p<0.05$) are shown.